CHALMERS
UNIVERSITY OF TECHNOLOGY

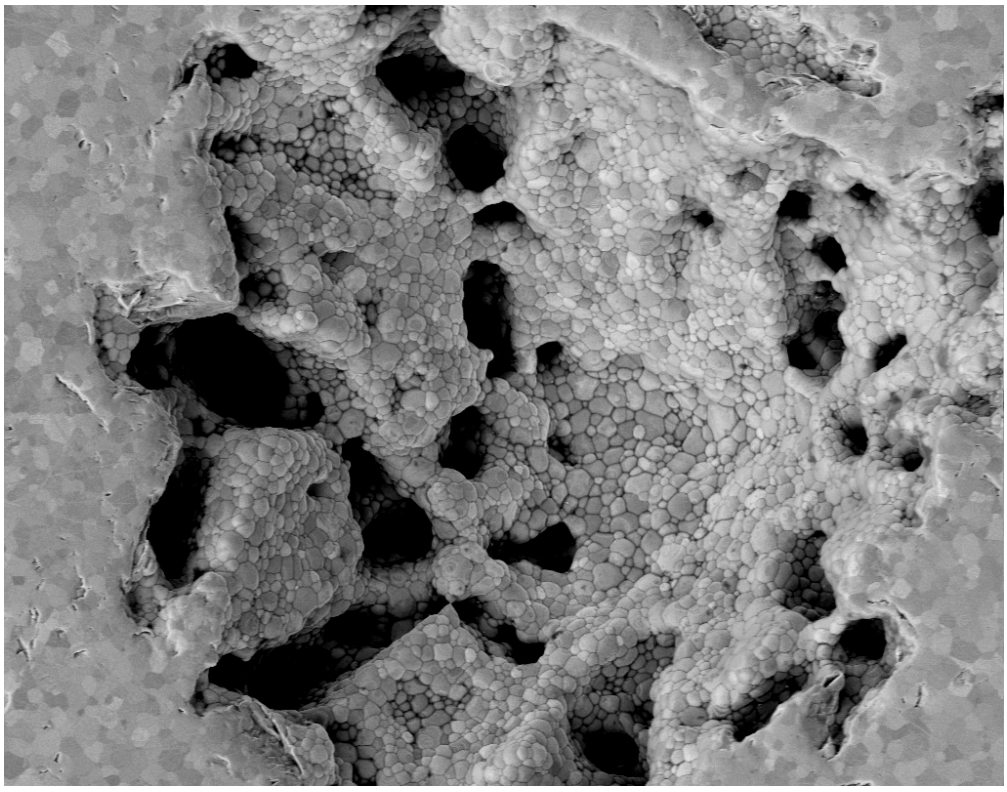

Synthesis and characterisation of nanometric simulated nuclear fuel (SIMfuel)

Making of Ln-doped nanometric SIMfuel through controlled co-precipitation of aqueous $Ln^{3+} - U^{4+}$

Master's thesis in Nuclear Chemistry

JULIA BERGSTRÖM

DEPARTMENT OF CHEMISTRY AND CHEMICAL ENGINEERING
CHALMERS UNIVERSITY OF TECHNOLOGY
Gothenburg, Sweden 2024
www.chalmers.se

Master's thesis 2024

Synthesis and characterisation of nanometric simulated nuclear fuel (SIMfuel)

Making of Ln-doped nanometric SIMfuel through controlled co-precipitation of aqueous $Ln^{3+}-U^{4+}$

JULIA BERGSTRÖM

CHALMERS
UNIVERSITY OF TECHNOLOGY

Department of Chemistry and Chemical Engineering
Division of Nuclear Chemistry
Chalmers University of Technology
Gothenburg, Sweden 2024

Synthesis and characterisation of nanometric simulated nuclear fuel
Making of Ln-doped nanometric SIMfuel through controlled co-precipitation of aqueous $Ln^{3+}-U^{4+}$
JULIA BERGSTRÖM

© JULIA BERGSTRÖM, 2024.

Supervisor: Marcus Hedberg, Department of Chemistry and Chemical Engineering
Examiner: Christian Ekberg, Department of Chemistry and Chemical Engineering

Master's Thesis 2024
Department of Chemistry and Chemical Engineering
Division of Nuclear Chemistry
Chalmers University of Technology
SE-412 96 Gothenburg
Telephone +46 31 772 1000

Cover: SEM image of nanometric La(III) and Ce(III) doped UO_2 pellet.

Typeset in LaTeX
Printed by Chalmers Reproservice
Gothenburg, Sweden 2024

Synthesis and analysis of simulated nanocrystalline nuclear fuel
Making of doped nanocrystalline SIMfuel through electrochemical reduction
JULIA BERGSTRÖM
Department of Chemistry and Chemical Engineering
Chalmers University of Technology

Abstract

In this project a procedure for the synthesis of Ce(III) and La(III) doped UO_2 SIMfuel was tested. The methods include electrochemical reduction of aqueous U(VI), Ln-doping, co-precipitation of nanometric doped UO_2 powder, and pressing and sintering of pellets. The aim was to synthesise SIMfuel with a high degree of dopant homogeneity and a nanometric grain structure found in irradiated uranium fuel with high burn-up structure. Four nanometric pellets were made, two with no dopants, one with 1% La, 1% Ce and one with 1% La, 5% Ce. Reference pellets were also made through U(VI) reduction in high temperature H_2 atmosphere. Elemental composition, unit cell dimensions, density, porosity, grain size and dopant homogeneity were characterised for nanometric pellets and reference pellets. Both types of pellets were found to have good homogeneity of dopants at both doping levels. The grain size for the nanometric pellets were found to not actually be nanometric, with a size range of around 1-25 µm. It is assumed that the high temperature sintering caused significant grain growth for the nanometric pellets.

Keywords: SIMfuel, Ln-doped UO2, electrochemical reduction, co-precipitation

Acknowledgements

I want to thank Marcus Hedberg for being an excellent supervisor and helping me learn through this experience. I want to thank Ivan Pidchenko from Studsvik Nuclear for teaching me about the electrochemical methods of creating SIMfuel and to let me borrow vital instrumentation. My heart goes out to all of the Nuclear Chemistry Department for having such a nice and welcoming work environment. I also want to thank Mustapha Saleh for lending me a hand so often during my work.

Julia Bergström, Gothenburg, June 2024

List of Acronyms

Below is the list of acronyms that have been used throughout this thesis listed in alphabetical order:

B1-B4	Uranium Electrochemical reduction Batch 1 to 4
BSE	Backscattered Electrons
CE	Counter Electrode
cps	Counts Per Second
EDX	Energy-Dispersive X-ray spectroscopy
FEG	Field Emission Gun
FP	Fission Products
HBS	High Burn-up Structure
ICP-MS	Inductively Coupled Plasma Mass Spectrometry
LA-ICP-MS	Laser Ablation Inductively Coupled Mass Plasma Spectrometry
LOM	Light Optical Microscopy
NM	Nanometric
NP	Nanoparticle
RE	Reference Electrode
SE	Secondary Electrons
SEM	Scanning Electron Microscopy
SHE	Standard Hydrogen Electrode
SIMfuel	Simulated irradiated nuclear fuel
UV-Vis	Ultraviolet-visible
WE	Working Electrode

Contents

List of Acronyms **ix**

1 Introduction **1**

2 Theory **3**
2.1 Nuclear reactors . . . 3
2.2 High Burn-up Structure . . . 4
2.3 SIMfuel . . . 5
2.4 Synthesis methods . . . 6
2.4.1 Electrolysis . . . 6
2.4.1.1 Electrochemical reduction of U(VI) . . . 7
2.4.2 Precipitation . . . 8
2.4.3 Vacuum filtration . . . 10
2.4.4 Pellet pressing and sintering . . . 10
2.5 Characterisation techniques . . . 11
2.5.1 Ultraviolet-visible (UV-Vis) spectroscopy . . . 11
2.5.1.1 Uranium light absorption . . . 12
2.5.2 Inductively coupled plasma mass spectrometry (ICP-MS) . . . 12
2.5.3 Helium Pycnometry . . . 13
2.5.4 X-ray diffraction (XRD) . . . 13
2.5.4.1 UO_2 unit cell . . . 14
2.5.5 Scanning Electron Microscopy (SEM) . . . 15
2.5.5.1 Energy-dispersive X-ray Spectroscopy (EDX) . . . 17

3 Methods **19**
3.1 Pellet Synthesis . . . 19
3.1.1 Glovebox handling . . . 19
3.1.2 Nanometric pellets . . . 19
3.1.2.1 Stock solutions . . . 20
3.1.2.2 Electrochemical reduction . . . 20
3.1.2.3 UV-Vis spectroscopy . . . 22
3.1.2.4 Precipitation . . . 22
3.1.2.5 Filtering and drying . . . 23
3.1.2.6 Powder grinding and pellet pressing . . . 24
3.1.2.7 Sintering . . . 24
3.1.3 Reference pellets . . . 25

3.2 Characterisation . . . 26
3.2.1 ICP-MS . . . 26
3.2.2 Pycnometry . . . 26
3.2.3 PXRD . . . 26
3.2.4 Pellet grinding and polishing . . . 27
3.2.5 LOM . . . 27
3.2.6 Pellet etching . . . 28
3.2.7 SEM and EDX . . . 28

4 Results and Discussion 29
4.1 Reduction of uranium . . . 29
4.2 Sintering and density . . . 29
4.2.1 Pycnometry . . . 32
4.3 ICP-MS data . . . 33
4.3.1 Stock solutions . . . 33
4.3.2 UO_2 powders . . . 33
4.4 PXRD data . . . 34
4.5 LOM imaging . . . 38
4.6 SEM imaging . . . 42
4.6.1 EDX . . . 44
4.7 Process difficulties and suggested improvements . . . 46
4.7.1 PTFE Contamination . . . 46
4.7.2 Wet powder . . . 47
4.7.3 Static charging . . . 48
4.7.4 Counter electrode vial . . . 48
4.7.5 Precipitation pH . . . 49

5 Conclusion 51

6 References 53

A Additional Pellet Data I

B Additional EDX scans III

C Electrolysis current graphs V

1

Introduction

Continued development in the field of nuclear chemistry is important for a multitude of reasons. From further improving upon the technology of operational or new nuclear reactors, to potential recycling of spent fuel and the final storage of highly radioactive waste. Most nuclear reactors use uranium dioxide pellets as fuel in the reactor core[1]. Over their lifetime in the reactor these fuel pellets develop new chemical and physical characteristics caused by the fission of uranium. These changes in characteristics include, among other things, new elemental composition, in the form of the fission products created from uranium, and crystallographic changes, such as increase in defects and reduction of grain sizes.

The large amount of various fission products in spent nuclear fuel makes it highly radioactive. This in combination with other factors such as restrictions on how nuclear fuel shall be handled and who can use it leads to it being rather difficult to study. An alternative would be to create synthetic spent nuclear fuel, called simulated irradiated nuclear fuel (SIMfuel). SIMfuel is made to mimic the properties of irradiated nuclear fuels while only containing stable isotopes of fission products and non-enriched uranium, making it much less radioactive and thus safer and easier to handle. The properties sought after in good SIMfuel should represent the properties of interest in a studied material. For this project those properties is a homogeneous mixture of the uranium and the fission product dopants, as well as a grain structure found in real fuel close to the rim.

SIMfuel is of specific interest to Studsvik Nuclear, a Swedish company working in the development of sustainable nuclear solutions. Their main interest in further development of SIMfuel is for the use as standards in laser ablation inductively coupled plasma mass spectrometry (LA-ICP-MS), which is a material analysis technique that uses a laser on a small area of the surface of a solid sample to ablate surface atoms for analysis. This instrument gives elemental composition of the sample with lateral surface resolution. Furthermore, good SIMfuel could be used in general research on spent fuel by any nuclear scientist in need. The problem lies in the synthesis of SIMfuel, as creating doped UO_2 with a similar grain structure to real fuel has proved to be rather difficult[2], [3].

This project aims to try a method of synthesising SIMfuel using electrochemical reduction of aqueous U(VI) into U(IV), followed by precipitation into nanometric UO_2 particles that are dried, pressed into pellets and sintered. The uranium will be doped with the fission products cerium and lanthanum in solution, before precipitation. Cerium is both a fission product in and of itself, as well as a commonly used

analog for plutonium. Lanthanum was primarily added as a reference. Only two fission products were chosen as this is primarily a test of the efficacy of the stated synthesis method.

The synthesised SIMfuel powders/pellets will be analysed using inductively coupled plasma mass spectrometry, pycnometry, X-ray diffraction, light optical microscopy, scanning electron microscopy and energy-dispersive X-ray spectroscopy. This will yield information about elemental composition, density, open porosity, lattice parameter, dopant homogeneity and grain size in sintered pellets. Some characteristics that could be important to know, but are not analysed in this project, include UO_2 particle size after precipitation and amount of oxygen relative to uranium and dopants.

2

Theory

This section will go over the theory behind this work as well as describe the methods used in the synthesis and characterisation, and describe the decisions made during the process.

2.1 Nuclear reactors

A conventional nuclear reactor generates electricity by boiling water that in turn spins a turbine driving a generator. The heat used to boil water originates from the fission of fissile radioactive nuclides such as U-235 and Pu-239[4] inside the reactor core. Inside the reactor core can be found the nuclear fuel, a moderator, a coolant and control rods. The control rods, made from a non-fissile material with a high neutron absorption cross section, controls the rate of fission in the fuel by changing the depth of insertion into the core. When inserted into the core, the control rods will absorb some of the neutrons instead of the fuel. The coolant cools the fuel by carrying away the heat to in turn boil the water that will spin the turbines. The moderator will slow down the neutrons generated by the fission reactions. Newly freed neutrons have high kinetic energy and are called fast neutrons. They are too fast to effectively get absorbed by fissile nuclides and must be slowed down, or loose kinetic energy, until they become so called thermal neutrons. This is achieved through scattering when colliding with the light atoms of the moderator. Water is used as both coolant and moderator in most reactors used today, like pressurized water reactors and boiling water reactors.[1]

The fuel used in most reactors is UO_2 pellets made from enriched uranium, containing 3-5% of the fissile U-235[4]. The pellets are stacked to form rods and put inside a cladding tube to physically separate the fuel from the coolant. Many fuel rods are assembled into an assembly, and multiple assemblies make up the reactor core. A single nuclear fuel pellet has a lifetime of around 3-6 years inside the core, before it must be taken out and either be recycled or disposed of. The fission reactions occurring inside the fuel pellets when in use have drastic effects that change the structure and elemental composition of the pellet.

2.2 High Burn-up Structure

High burn-up structure (HBS) is the name given to the unique structure exhibited by spent UO_2 nuclear fuel pellets in light water reactors. Fuel pellets inside operating reactor cores will significantly change their chemical and structural properties over the course of their lifetimes. Figure 2.1 shows a schematic cross-section of a spent fuel pellet exhibiting HBS. The characteristics of HBS include a reduction of grain size with increasing distance from pellet center. Before use the pellet has a homogeneous grain structure, with grain sizes similar to the center of the pellet in the figure, across the entire pellet. Over time in the reactor core the larger grains on the rim of the pellet will break apart into smaller grains because of stress and damage from the fission occurring in the pellet. The reason for a grain size gradient is twofold. The rim of the pellet will experience more fission than the inside, as thermal neutrons coming from the moderator has a higher likelihood of reacting with fissile atoms at the rim, with a diminishing amount of fission further towards the center. The second reason for the size gradient is a temperature gradient in the pellet. UO_2 is a rather poor thermal conductor and therefor the pellet will have a much higher temperature in the middle than on the rim, with ca. 1300-1500 K at the centre and ca. 600-800 K at the rim[5]. This means that any smaller grains towards the pellet centre will combine into larger grains because of the high temperature. The grain size gradient can be seen with the 5 images in the lower left of Figure 2.1, with the different colors representing different crystal planes.

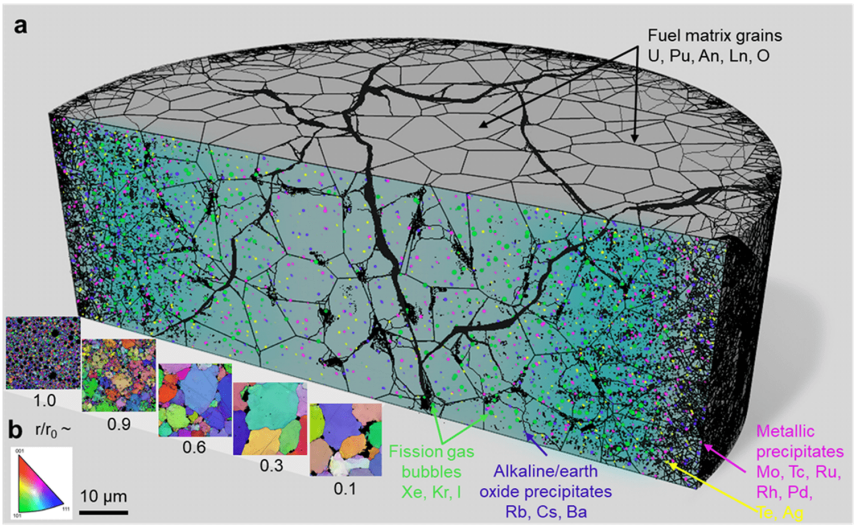

Figure 2.1: Schematic cross-section of a UO_2 fuel pellet with a high burn-up structure. Figure reproduced from Mao et al. [6].

Another important property of spent nuclear fuel are the fission products (FP). FP are the new elements formed during the fission of a fissile elements like U-235. Around 30 different FP elements can be found in spent nuclear fuel, which can be divided into 4 categories[7]:

- Volatile FP, i.e. noble gases and halogens

- Metallic precipitates, e.g. Mo, Tc, Ru
- Ceramic precipitates, e.g. Rb, Cs
- Soluble FP, e.g. Y, La, Ce

The fission gases accumulate into small gas bubbles inside the pellet, while the non-soluble solids can form metallic or ceramic aggregates. The elements that can be dissolved in the UO_2 crystal structure includes mostly lanthanides. These will, because of the random nature of fission, be homogeneously distributed in the fuel matrix at a given radial distance. Although a FP radial gradient will be present because of the same reasons that give rise to the grain size gradient. Firstly, more fission at the rim leads to a higher initial amount of FP. Secondly, the temperature gradient present causes FP to diffuse preferentially in the direction of decreasing temperature, as diffusion increases with increasing temperature, and vice versa.

2.3 SIMfuel

Simulated irradiated nuclear fuel, or SIMfuel, is material made to mimic the characteristics of real spent nuclear fuel as described above, while only containing stable isotopes of the FP. There are a few reasons of interest in making SIMfuel. Spent nuclear fuel is highly radioactive and therefor difficult and potentially dangerous to handle. It is therefor no easy task to analyze and conduct experiments on spent fuel. SIMfuel that consists of non-enriched UO_2 and stable FP isotopes is significantly less radioactive and by comparison much sader and easier to handle. In using SIMfuel it is also possible to study the effects a single, or a few, FP have on the fuel, by selectively choosing which FP to use as dopants. SIMfuel that adequately mimics the HBS can be used as a replacement of real fuel in experiments or as standards for the analysis of real fuel, among other things.

It is however difficult to mimic the properties of HBS in SIMfuel. Previous works at Chalmers by H. Oliva[2] and I. Lundell & S. Ekman[3] have shown that getting a sufficiently homogeneous distribution of dissolvable FP in a UO_2 pellet is possible with relatively east methods, while the nanometric (NM) grain structure of the HBS rim is much harder to replicate. The most reasonable way to create a NM pellet would be to make it from a NM powder. This is not possible with the primary method used by both mentioned works, as it requires reduction of solid U(VI) into U(IV) by heating in the presence H_2, where the high temperatures would make any NM powder grow to a larger size. Therefor another method for the making of U(IV), or UO_2, which allows the creation of NM UO_2 particles is needed. One possible method is the electrochemical reduction of uranium in aqueous solution, followed by slow precipitation, producing NM powder.

It was decided that three types of NM SIMfuel was to be made in this project: undoped UO_2, UO_2 doped with 1% La and 1% Ce, and UO_2 doped with 1% La and 5% Ce. Lanthanum was chosen primarily as an internal standard to be able to easily compare the pellets with other doped pellets in the future. Lanthanum is also one of the FP found in spent fuel. Cerium is also a FP in spent fuel, but it was chosen primarily because it is often used as a non-radioactive analog for plutonium[8]. The

1% cerium was chosen because that is the amount of plutonium usually found in spent fuel[4]. Meanwhile 5% cerium was chosen because it is easier to characterize a larger amount of dopant and to see if homogeneity and grain size is affected by a higher dopant level.

2.4 Synthesis methods

2.4.1 Electrolysis

An electrochemical setup normally includes three electrodes in an electrolyte, connected by wires to a power source. The electrolyte is an ion conducting liquid, often H_2O with salts or other charged species such as acids. Electrochemical reactions occur on two of the electrodes. When a potential is applied over these electrodes one of them will act as the working electrode (WE) and the other as the counter electrode (CE), depending on the sign, or "direction", of the potential. Electrons will flow from the CE to the WE through the metallic connection (wires), while a positive ion, often H^+, flows from the CE to the WE through the electrolyte, thus completing the electric circuit. At the WE, also known as the cathode, some species in the electrolyte will pick up an electron and decrease its oxidation state, known as reduction. At the CE, also known as the anode, another species will donate an electron, which travels to the WE, and increase its oxidation state, known as oxidation.

Oxidation state is essentially the same thing as the charge of an ion. For example an ion with oxidation state 3 has a charge of +3. For metallic elements the oxidation state is often denoted with roman numerals, e.g. Fe^{3+} becomes Fe(III).

A simple example of electrolysis is the reduction and subsequent oxidation of acidic water. At the WE, hydrogen ions will be reduced and create hydrogen gas:

$$2\,H^+ + 2\,e^- \longrightarrow H_2$$

While on the CE, water will be oxidised into oxygen gas and hydrogen ions:

$$2\,H_2O \longrightarrow O_2 + 4\,H^+ + 4\,e^-$$

The first reaction is called the reduction half-reaction and the second is called the oxidation half-reaction. Combining the two half-reactions gives the full reaction, called a redox reaction:

$$2\,H_2O \longrightarrow O_2 + 2\,H_2$$

Any electrochemical reaction needs a certain potential to start. Tabulated potentials for reduction half-reactions are known as standard electrode potentials (E°), where difficult to reduce species such as Li^+ have low/negative values, while easy to reduce species such as Au^+ have high positive values. This also means that the

corresponding reversed oxidation half-reaction is favourable with a low E°and unfavourable with a high E°, such as the oxidation of Li and Au respectively. Electric potential is not an absolute value such as electric current, there is no universal 0 potential. Potential must therefor be compared to something when measured in electrochemistry. The most common scale is called the Standard Hydrogen Electrode (SHE) and sets the previously mentioned reduction half-reaction of H^+ into H_2 as the zero value. Other scales can be converted between each other linearly by adding or subtracting corresponding conversion values.

The third electrode in the setup, the reference electrode (RE), is used to measure the applied potential. To do this a more sophisticated instrument must be used in the place of a power source, such as a potentiostat that is able to measure and apply specific potentials. The RE is added into the electrolyte together with the other two electrodes and connected to the potentiostat. The applied potential is now relative to the RE used. For example an applied potential of 0 V using a Ag/AgCl RE, denoted 0 V vs Ag/AgCl, will not be the same as 0 V vs SHE, but rather equals +0.197 V vs SHE[9].

2.4.1.1 Electrochemical reduction of U(VI)

Uranium has two common oxidation states, U(IV) and U(VI). Unless kept stable by e.g. being in a large UO_2 crystal, U(IV) will readily oxidize up to U(VI). Dissolved aqueous U(IV) or nanometric U(IV) with large surface to volume ratio will oxidize in the presence of oxygen.

Figure 2.2 shows an electrochemical cell used in this work. This cell consists of a glass beaker containing the uranium solution acting as the electrolyte, a WE, RE, a stir bar, and a vial with a porous glass frit containing the CE.

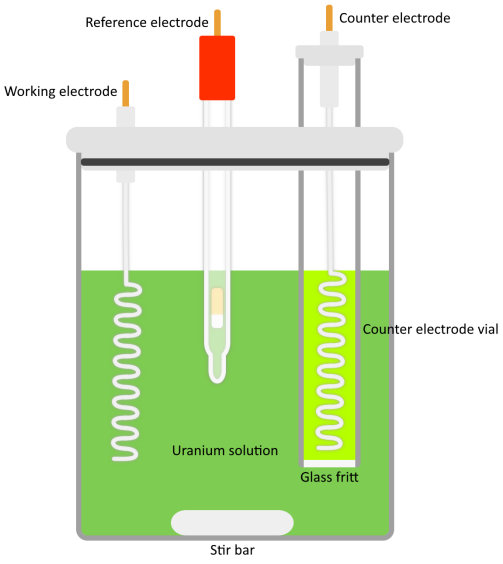

Figure 2.2: A 3-electrode electrochemical setup for aqueous uranium reduction.

The following reactions describe what happens in the cell during the reduction of

U(VI) into U(IV). Equation 2.1 is the half-reaction occurring on the WE where the uranium is reduced. Aqueous $U(VI)O_2^{2+}$ species comes into contact with the surface of the WE, receives two electrons and forms U(IV), while H^+ binds with the O^{2-} to form H_2O. At the same time half-reaction Equation 2.2 occurs on the CE, where H_2O is oxidized, turning into H^+ ions and O_2 gas, while donating electrons to the CE. If U(IV) comes into contact with the CE it will oxidize back into U(VI), therefor the CE is separated from the bulk solution using the vial. The vial also prevents the oxygen generated on the CE from going into the bulk solution, which would also cause U(IV) to oxidize back into U(VI). The CE vial is capped at the end with a porous glass frit that allows H^+ diffusion from the vial into the bulk solution, thus completing the electric circuit with H^+ moving from the CE to the WE.

$$UO_2^{2+} + 4\,H^+ + 2\,e^- \rightleftharpoons U^{4+} + 2\,H_2O \tag{2.1}$$

$$2\,H_2O \rightleftharpoons 4\,H^+ + 4\,e^- + O_2 \tag{2.2}$$

$$2\,UO_2^{2+} + 4\,H^+ \rightleftharpoons 2\,U^{4+} + 2\,H_2O + O_2 \tag{2.3}$$

Finally Equation 2.3 shows the full redox reaction of the combined half-reactions. The cell has a net loss of U(VI) and H^+, and a net gain of U(IV), H_2O and O_2. The consumption of H^+ means that the pH of the solution is increasing during operation, but the total change in pH is negligible with if the uranium concentration is low enough. The generated oxygen goes out through the top of the anode vial into the surrounding atmosphere and, given that the setup is positioned inside an inert atmosphere glovebox, will be removed by the glovebox's oxygen filtering system.

2.4.2 Precipitation

U(VI) and U(IV) can be dissolved in low pH aqueous solution, while at higher pH the U(IV) will precipitate out of solution as UO_2. The precipitation of U(IV) follows Equation 2.4, where the dissolved U(IV) reacts with OH^- to form solid UO_2 precipitate particles and H_2O.

$$U^{4+} + 4\,OH^- \rightleftharpoons UO_2 + 2\,H_2O \tag{2.4}$$

When precipitating U(IV), the speed of pH increase will greatly determine the structure of the solid uranium precipitate. A fast pH change will lead to an amorphous phase, while a slower increase will give a crystalline phase. If the pH is increased slowly this will produce NM uranium particles.

Solubility lines for U(IV) and U(VI) are shown in Figure 2.3. Any U(IV) solution with conditions between the $U(IV)O_2(cr)$ and $U(IV)O_2 \cdot H_2O(am)$ lines will precipitate out crystalline UO_2, while above the amorphous line the precipitates will be amorphous. The graph also has experimental data points, with four points showing the size of precipitated particles at the given conditions. So if the pH of a U(IV) solution is brought into the crystalline precipitation region, the uranium will precipitate as UO_2 nanoparticles (NPs). If however the pH is brought up further into the amorphous region, a majority of the precipitate will be amorphous UO_2. Although

the pH will pass through the crystalline region, the slow speed of crystal formation and/or growth will mean that not many UO_2 crystals are formed if the pH is raised at a fast speed. However when UO_2(cr) has formed it will stay crystalline at higher pH values.

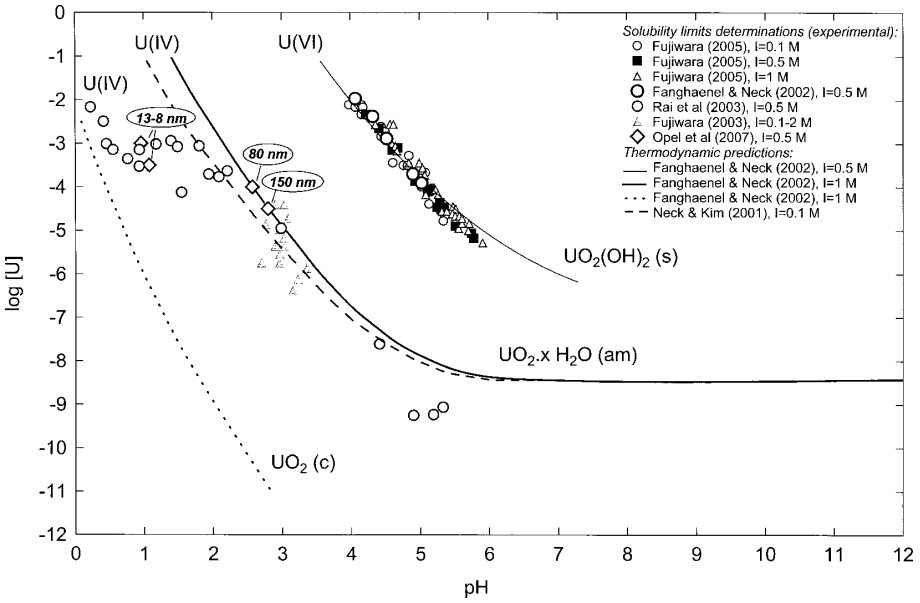

Figure 2.3: Graph showing theoretical solubility limits, together with experimental data, for U(IV) and U(VI) in aqueous solution. Figure reproduced from Gil et al.[10].

The base needs to be added slowly when increasing the pH value into the crystalline region. This is because when added, the base will take some amount of time to dissolve homogeneously into the bulk solution. Directly after addition, any U(IV) in the temporary high pH volume surrounding the base droplet can form amorphous UO_2. To minimize the amount of amorphous UO_2, the base is added one drop at a time with a high stir speed applied to the solution. The four data points in the graph that do show particle sizes show an increase of size with increased pH, which is another reason to precipitate at lower pH values if NPs are desired.

Figure 2.4 shows a pourbaix diagram for both cerium and lanthanum in aqueous perchlorate and water, respectively. It can be seen that Ce(III) remains dissolved from pH 4 up to pH 9.5 in the water stability region (between the negative sloped dotted lines). La(III) remains dissolved up to pH 7.5-9.5, depending on concentration. Therefor when precipitating Ce and La doped uranium the pH should be brought up to around these pH values to be sure that everything has precipitated. Although if the Ce and La does not precipitate together with the U at pH 1-2, the dopants will not be homogeneously distributed. Another reason for bringing up the pH to above 7 is that the precipitated particles will start aggregate at higher values, which will make it easier to filter and handle when fully dried.

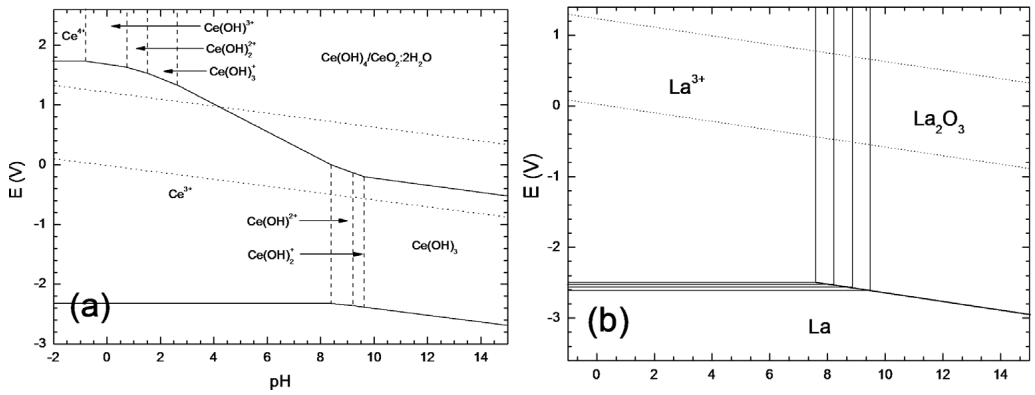

Figure 2.4: Pourbaix diagram for cerium in aqueous perchlorate (left) and lanthanum in water (right). Unknown concentrations. Figure reproduced from Um.[11].

2.4.3 Vacuum filtration

A method to quickly separate the bulk of a liquid from solid particles is through filtration. Vacuum filtration works by pouring the supernate liquid and precipitate particles onto a filter paper inside a funnel. A vacuum is applied on the other side of the filter paper using e.g. a vacuum ejector or pump. The vacuum suck the liquid through the filter, leaving the particles behind, given that the filter pore size is smaller than the particles. The now moist particles can be taken out of the funnel and be dried fully either in open air or inside a desiccator.

2.4.4 Pellet pressing and sintering

Powder is added into a pressing die, a cylindrical mold with two movable pressing rods on either side of the powder. The die is put inside a pressing machine that applies a large force on the pressing rods. Even hand-operated presses can apply forces of multiple tons onto a pellet area of often below 1 cm. A fine powder must be used to press good pellets, therefor any aggregated powder must be ground down using e.g. a mortar and pestle or grinding machine. Otherwise any larger and harder aggregates might not break apart during pressing and form a more rough pellet surface. After pressing at sufficient pressure the newly formed pellet will hold together but can still break if handled too roughly.

Sintering is a technique where a solid material is heated inside a furnace at a high temperature, which is below the melting point of the material, to increase the density of the material. The high temperature allows the particles of the pressed pellet to compact through surface and bulk transport, lowering their surface energy. This means that smaller particles, which have a higher surface area compared to larger particles of the same volume, will sinter faster.[12] The result is a reduction in porosity and stronger binding between particles, which during sintering turn into grains of the crystal. The sintering process will also increase the grain size.

A method for sintering UO_2 is to put the pellets in crucibles capable of handling high temperatures, and inserting into a furnace. When heating up to the maximum chosen temperature, the rate of heating needs to be considered. NM UO_2 made from

the electrochemical precipitation method will have some amount of water bound to the large surface area of the pressed pellet. If the temperature is raised too quickly around 100 °C the water could vaporize violently, causing cracking in the pellet. Other impurities or possibly properties of the material, such as thermal expansion, could also affect the pellet negatively if the heating rate is too fast. After reaching the maximum temperature the furnace holds for a determined amount of time before cooling down to room temperature at a similarly cautious rate.

A gas mixture flow of inert and reducing gases, such as a noble gas and H_2 needs to be applied inside the furnace when sintering UO_2, or anything else that can react with O_2. Even though the pressed UO_2 pellet is kinetically stable to oxygen at room temperature, it will react at higher temperatures. The H_2 is added to the gas to reduce any possible U(V) and U(VI) in the pellet.

2.5 Characterisation techniques

2.5.1 Ultraviolet-visible (UV-Vis) spectroscopy

UV-Vis spectroscopy is a non-destructive analysis technique used to gain information about a sample's light absorption capabilities. The sample is diluted in a liquid with low absorption, in a small glass cuvette, and placed inside the UV-Vis spectrophotometer. Inside is a light source and a wavelength selector, capable of emitting selective wavelengths of light from ultra violet to visible light, and often into the near infrared region as well. The monochromatic light is shone on the sample and, optionally, a reference cuvette containing pure dilution liquid. The light passes through both cuvettes and a detector on the other side measures the intensity of the light that passes through. Thus, if a spectrum of many wavelengths are analysed, an absorption spectrum graph can be made by plotting the inverse of the light intensity over wavelength. The absorption spectrum from the reference sample is subtracted from the main sample spectrum. Absorption spectra are unique for each type of sample and can be used as identification.[13] Also, different oxidation states of the same element have different spectra, and thus UV-Vis can be used to differentiate between U(VI) and U(IV).

The height of absorption peaks are dependent on the amount of sample in the analysis cuvette, which means that UV-Vis can also be used for concentration analysis. All absorption peaks for all types of samples have a so called extinction coefficient which can be used to convert absorption to concentration using Beer-Lamberts law:[13]

$$A = \varepsilon l c \tag{2.5}$$

Where A is the absorption, ε is the extinction/absorption coefficient, l is the optical path length (which is usually equal to 1), and c is the concentration. However, the relationship between concentration and absorbance is only linear up to a certain concentration, after which Equation 2.5 stops working.

2.5.1.1 Uranium light absorption

Figure 2.5 shows the absorption spectra for both U(VI) (blue) and U(IV) (red). The U(VI) "zero line" on the right is raised compared to the U(IV) zero line on the left, because U(VI) has no reference sample. As can be seen, the two spectra are distinct and can mostly be easily differentiated. The U(IV) left most peak does overlap with the most prominent U(VI) peaks, which makes it harder to differentiate the two spectra when the U(IV) absorption is higher than that of U(VI). When UV-Vis is used to see if there is any significant amount of U(VI) remaining after electrolysis, it is therefor best to use the left most peaks of the U(VI).

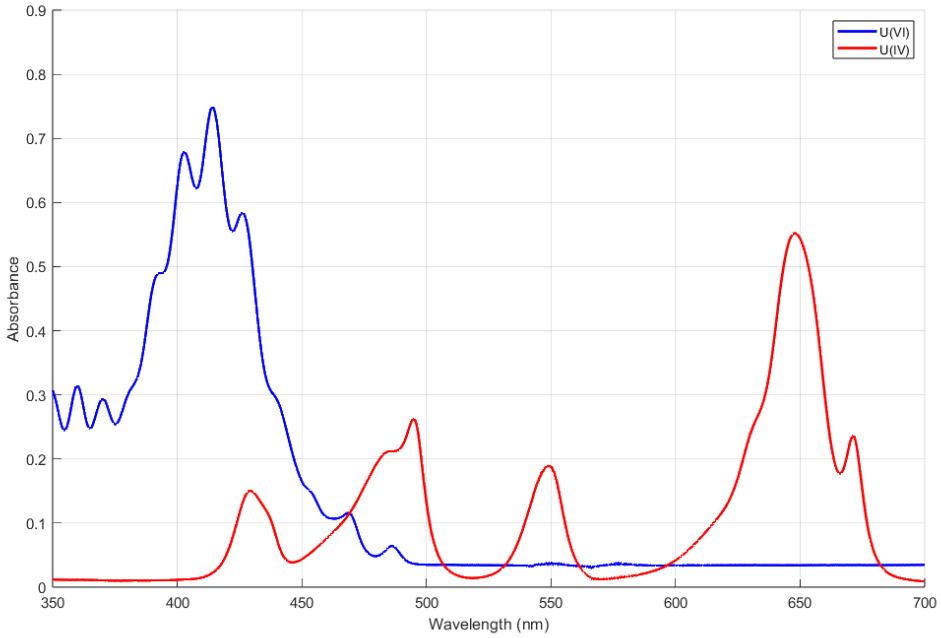

Figure 2.5: Absorption spectra for U(VI) (blue) and U(IV) (red) in 1 M $HClO_4$(aq). U(VI) has a concentration of 0.09 M, and no reference sample. U(IV) has a concentration of 0.009 M, with a 1 M $HClO_4$(aq) reference sample.

2.5.2 Inductively coupled plasma mass spectrometry (ICP-MS)

ICP-MS is a sensitive mass spectroscopy technique used for the detection and quantification of atoms in a sample. The measured sample is most often dissolved in a liquid, and diluted down to the range of atomic ppb, so as to not overwhelm or damage the detector. The sample can for example be dissolved in water or an acid such as HNO_3. The sample liquid is pumped into the instrument where the ICP breaks it down into its atomic constituents which are then also ionized. The ICP uses an induction coil to turn argon gas into a plasma, which in turn ionizes the sample. The ions then move into the MS, which works like an ordinary mass spectrometer and typically consists of an ion focusing lens, a quadrupole mass filter, and a detector. The quadrupole filters out the ion masses selected by the operator

to be analyzed, which move to the detector which measures the ions in counts per time unit. An ICP-MS is sensitive enough to distinguish between different isotopes of the same element.[14]

To turn the counts detected by the instrument into concentration of the sample, a series of standards must be used. The standards contain a known amount of the elements that are to be measured, with a concentration range around what the sample is expected to have. The standards are measured at right before the sample(s), and their counts per second (cps) results are used to graph the linear relationship between cps and concentration.

2.5.3 Helium Pycnometry

Pycnometry is a technique used for the measurement of solid sample volume. It measures the volume of the solid material together with the volume of any closed pores inside the material. Closed pores are volumes of open space in the sample which are completely closed off from the outside. Helium pycnometry specifically uses He gas to measure sample volume, using the pressure-gas relationship of Boyle's law. The sample is placed inside a sealed container with known volume, and He gas is pumped in. The instrument then measures the pressure in the container after pumping in a known amount of He. The pressure is then converted into sample volume. The reason closed pore volumes are added to the sample volume is because the He gas can't go through the solid sample walls.[15]

The measured volume of a sample can vary from day to day. A standard with a known volume is therefor measured before the sample(s), and the difference between the measured volume and actual volume of the standard is later used to correct the error in the sample's measured volume.

2.5.4 X-ray diffraction (XRD)

There are two general types of XRD; single crystal XRD, and powder XRD (PXRD), which was the type used in this work. PXRD is a technique used to analyze crystalline powder. The information gained include the structure and size of the crystal unit cell, presented in the way of X-ray diffractograms. Diffractograms show counts per second over the measured angles, 2θ.

A PXRD instrument works by shooting a monochromatic (though in reality it is often a bit more than one) X-ray at the powder sample. The X-rays are reflected on the sample and travel up into a detector that measures the intensity of reflected X-rays, in the form of counts per second. The way X-rays interact with crystalline materials means that constructive or destructive interference occurs, leading to variation in the intensity of reflected light reaching the detector. As such, during a measurement, the angle of the X-ray source, and detector, is varied from low to high, or vice versa. This creates the aforementioned diffractograms, where only certain angles, dependent on the structure of the sample, will show constructive interference and create a peak in the diffractogram.[16] Figure 2.6 shows two X-rays reflecting off of two adjacent crystal planes at an angle which allows for constructive interference.

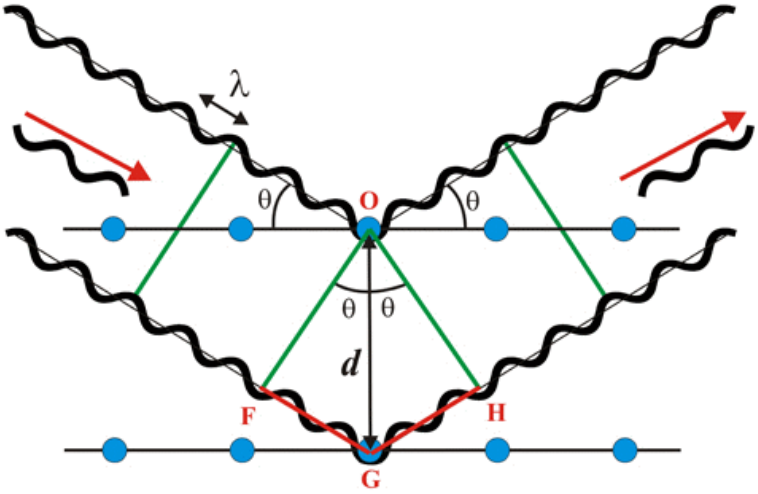

Figure 2.6: Image showing Bragg reflection from crystal planes with constructive interference. Blue dots are atoms, d is the atomic interplanar spacing and θ is the incident angle.[17]

Constructive interference only occurs when the difference in path length for the X-rays, F to G to H in the figure, is equal to the X-ray wavelength times an integer. An equation for where constructive interference occurs can be summarised with the Bragg equation:[16]

$$n\lambda = 2d_{hkl}sin(\theta_{hkl}) \tag{2.6}$$

Where n is and integer, λ is the X-ray wavelength, d is the interplanar spacing, θ is the incident angle (or Bragg angle) and the subscripts hkl are the miller indices, integers used to define specific atomic planes. A second equation exists to calculate unit cell dimension, or lattice parameter, for cubic unit cells:[16]

$$d_{hkl} = \frac{a}{\sqrt{h^2 + k^2 + l^2}} \tag{2.7}$$

Where a is the lattice parameter. With these two equations it is possible to use the data from PXRD, diffraction peak angles θ, to calculate the lattice parameter, given that the unit cell is cubic and that the miller indices for each peak is known.

2.5.4.1 UO_2 unit cell

UO_2 is a crystalline material with a face centered cubic $fm\bar{3}m$ "fluorite structure" unit cell.[18] Figure 2.7 shows the unit cell for UO_2, where the gray atoms are U and the red atoms are O. The exact lattice parameter for UO_2 varies with the amount of oxygen, as real UO_2 is often slightly oxidised into UO_{2+x}, where x<1. There also appears to be various studies that report different lattice parameters independent of oxygen fraction. A study claiming to have accurately measured the lattice parameter puts it at 5.47127±0.00008 Å at 20 °C for $UO_{2.000\pm0.001}$.[19]

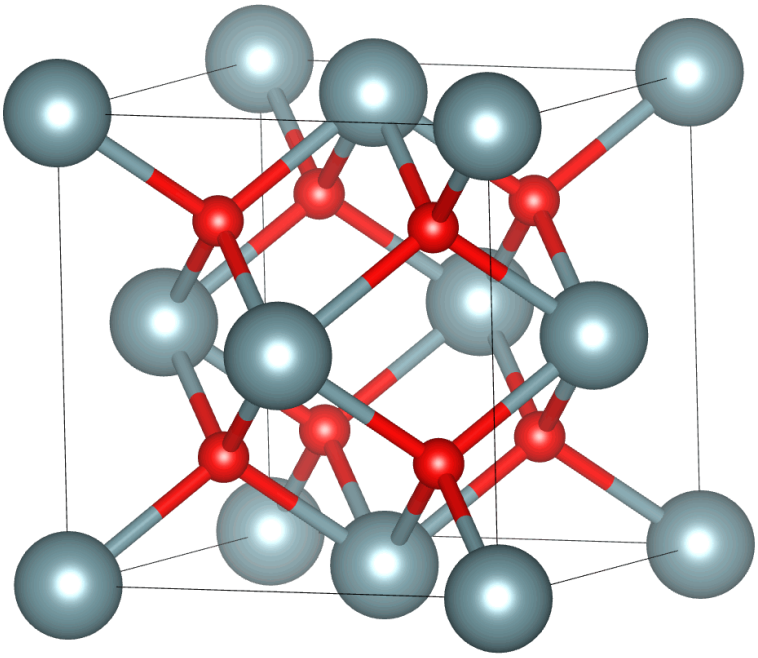

Figure 2.7: Unit cell for UO_2. Gray atoms are uranium and red atoms are oxygen.

When UO_2 is doped with Ce and La, or any other dissolvable element, the lattice parameter will change. Doped Ce or La will occupy a position normally taken by U in the unit cell. The size of the dopants relative to U will determine if the unit cell will expand or contract. Table 2.1 shows the ionic radii of U, Ce, La and O as they would be in a UO_2 unit cell. UO_2 doped with Ce(IV) would shrink in size as Ce(IV) is smaller than U(IV), and they have the same oxidation state. This has also been shown experimentally.[20]

For La(III) doping the system must be charge balanced as La(III) has a lower oxidation state than U(IV). This could occur through the creation of O vacancies, or the oxidation of U(IV) into U(V) and/or U(VI). If O vacancies occur, the lattice parameter should decrease since the size of O(-II) is larger than two times the difference between U(IV) and La(III) (one O vacancy for every two La). On the other hand if instead U(IV) is oxidised then should the lattice parameter increase since La(III) is larger than both U(IV) and U(VI). Experimental results show that La doping increases the lattice parameter of UO_2[21].

Ce(III) doping would likely act similar to La(III) doping, if it weren't for the fact that Ce(III) could possible oxidise to Ce(IV). Experimental results have shown that Ce(III) doping affects the lattice parameter in a similar manner to Ce(IV), that is decreasing the parameter[22]. It is therefor possible that most Ce(III) oxidises into Ce(IV).

2.5.5 Scanning Electron Microscopy (SEM)

Scanning Electron Microscopy by Nanoscience Instruments[24] was used as source for the following section.

Table 2.1: Ionic radii for 8-coordinate U, Ce, La, and 4-coordinate O.[23]

Species	**Ionic radii in UO2 unit cell [pm]**
U(IV)	114
U(VI)	100
Ce(III)	128.3
Ce(IV)	111
La(III)	130.0
O(-II)	124

SEM is a microscopy technique with better resolution than normal light microscopes, down to 1 nm for the best SEMs. It is used to image small sample details and roughly differentiate between different elements, among other things. An SEM uses high energy (high speed) electrons, instead of photons, to image a surface. Electrons with sufficiently high kinetic energy, or accelerating voltage, will have a wavelength smaller than visible light. At, for example, an accelerating voltage of 10 kV, the electrons will have a wavelength of 0.0122 nm, compared to the 400-700 nm range of visible light.

An electron source (or gun), which emits the electrons. There are a few types of electron sources, including a tungsten filament, a solid-state hexaboride crystal and a field emission gun (FEG). A FEG is a tungsten wire ending in a sharp tip. An applied electric field is used to accelerate electrons towards the tip, while another field applied to the FEG tip extracts the electrons through electron tunneling.

A set of electromagnetic lenses reduce the diameter of the electron beam, and finally focuses the electrons on a small spot on the surface. Scanning coils are then used to deflect the beam so that it moves across the surface in a raster scan motion.

Most SEMs have two electron detectors to detect the two "important" types of electrons emitted from the sample surface, backscattered electrons (BSE) and secondary electrons (SE). BSE are electrons from the electron gun that enter the sample and are scattered back out by flying close enough to the nucleus of a sample to turn around ca. 180°. Using BSE it is possible to differentiate between elements with a larger mass difference, as an atom with more protons will scatter more electrons than one with fewer protons. The SE come from the primary electrons knocking out an electron from a sample atom, which then goes out of the sample. An intrinsic difference between BSE and SE is that the BSE will have higher kinetic energy than the SE. It is therefor possible to separate them by applying a field that will bend the path of the SE to the side, while the path of the faster BSE is not affected as much.

Because BSE have a higher energy they, manage to come back out of the sample from a deeper inside than SE, called penetration depth. Furthermore, since the primary electrons entering the sample spread out the further down they go, creating a droplet shape in the sample, BSE electrons originate from a larger surface area than SE. SE therefor give better surface resolution and topographical information than BSE. The sample needs to be electrically conductive to some degree, as otherwise electrons will

build up on the sample during measurement.

Finally the data collected by the detectors are sent to a computer that reconstructs it into an image, where points with a high electron emission are colored more white while points with low electron emission are colored more black/dark. This creates a black and white image of the sample surface.

The last vital component of the instrument is a vacuum pump. The primary purpose is to protect the electron gun, as it would be damaged if it were turned on without a vacuum. The level of the vacuum therefor needs to increase with a higher accelerating voltage. Another reason for the vacuum is to prevent electrons from interacting with anything other than the sample.

2.5.5.1 Energy-dispersive X-ray Spectroscopy (EDX)

EDX, also known as EDS, is another analysis technique that is integrated into many SEM instruments. It is used to characterise the elemental composition of the sample surface. When a SE is emitted from an atom, an electron from a higher orbital will fall down to fill the vacant spot, and in the process an X-ray will be emitted. Emitted X-rays are characteristic to whatever element emitted them, and as such can be used to determine the elemental composition of the sample. A SEM capable of EDX will also have a detector for X-rays, capable of differentiating between different wavelengths and measuring their intensity. An intensity over wavelength graph is made for any point analysed, and peaks are compared to a database with the characteristic wavelengths for all elements. This then gives the atomic composition of the analysed point. Like SEM imaging, multiple points can scanned to analyse for example single lines or an area.

3
Methods

3.1 Pellet Synthesis

In total seven different pellets were made using two methods; the electrochemical reduction method, yielding nanometric UO_2 powders/pellets, and the standard "ADU" method. The ADU pellets were made as a reference to compare with the nanometric pellets made from the electrochemical reduction method.

Four NM pellets were made, two with 100% U, one doped with 1% La(III) and 1% Ce(III), and one doped with 1% La(III) and 5% Ce(III). The three reference pellets were made with 100% U, 1% Ce(III) doping and 5% Ce(III) doping, respectively.

The method for making the NM pellets used in this project largely follows the methods presented in R. Jovani-Abril's dissertation on the making of NM UO_2 [25].

3.1.1 Glovebox handling

The entire NM pellet synthesis up to and including pellet pressing was performed in inert atmosphere so as to not oxidize the NM uranium. All steps, excluding pellet pressing, were performed inside a positive pressure glovebox with an N_2 inert gas atmosphere with 0.1 ppm O_2. The amount of oxygen could usually go up to 0.7 ppm during use, and a few times went temporarily higher (maximum recorded was 10.6 ppm) because of minor incidents such as bringing in sealed containers containing standard atmosphere.

To take items into a glovebox they must go through a vacuum airlock antechamber to bring oxygen levels down to the same level as in the glovebox. The procedure for items that can handle full vacuum is to bring down to "full" vacuum (-100 kPa) and back up to glovebox pressure (flushing) three times before bringing in the item. For items that can not handle full vacuum or might be damaged such as liquids or electronics, the general procedure is to flush down to -90 kPa 7-8 times.

3.1.2 Nanometric pellets

U(VI) was reduced in a perchloric acid solution to U(IV) through electrochemical reduction, precipitated using ammonium hydroxide, filtered and dried, pressed into pellets and then sintered in a tube furnace.

3.1.2.1 Stock solutions

A 0.1 M U(VI) stock solution was prepared by adding 23.92 ml of 2.09 M $UO_2(NO_3)_2 \cdot 6\,H_2O$ in two centrifuge tubes filled with concentrated ammonium hydroxide (NH_3(aq)). The tubes were centrifuges at 4000 rpm for 5 min. The NH_3(aq) was decanted leaving the solid uranium precipitate in the tubes. The tubes were washed with MQ water and centrifuged again at the same settings, and the water was decanted. The precipitate was added to a beaker with 500 ml of 1 M perchloric acid ($HClO_4$(aq)), and was stirred and heated until it dissolved.

A 50 mM Ce(III) stock solution was made by adding 2.1870 g of $Ce(NO_3)_3 \cdot 6\,H_2O$ directly to 100 ml of 1 M $HClO_4$(aq).

A 50 mM La(III) stock solution was made by adding 2.1598 g of $La(NO_3)_3 \cdot 6\,H_2O$ directly to 100 ml of 1 M $HClO_4$(aq).

Inductively coupled plasma mass spectrometry (ICP-MS) was performed on all stock solutions to determine more accurately the final concentrations. The concentrations for the uranium, cerium and lanthanum stock solutions were measured to be 91.9 mM, 33.7 mM and 42.6 mM respectively.

All stock solutions and other liquids such as MQ water and 1 M $HClO_4$(aq) was bubbled with N_2 gas for around 20-30 minutes depending on volume, so as to remove dissolved O_2 in the liquids, before they were moved into the glovebox.

3.1.2.2 Electrochemical reduction

A Metrohm DropSens μStat-i 400s was used for the electrochemical reduction. A saturated calomel electrode (SCE) was used as the reference electrode and a Pt spiral electrode was used as counter electrode. For working electrode a reticulated vitreous carbon electrode (or glassy carbon foam electrode) was used for the first reduction but reduction batches 2-4 used a Pt spiral electrode as working electrode. A ca. 100 ml glass beaker with accompanying lid and a stir bar was used for the reduction. All electrodes were generally inserted as deep into the solution as possible without hitting the stir bar. The counter electrode was furthermore put inside a smaller glass vial with a glass frit at the end, so as to both prevent generated oxygen from going into the bulk solution and prevent U(IV) from re-oxidising at the counter electrode, while still allowing a flow H^+ between electrodes. Figure 3.1 shows the setup with the two different working electrodes that were used.

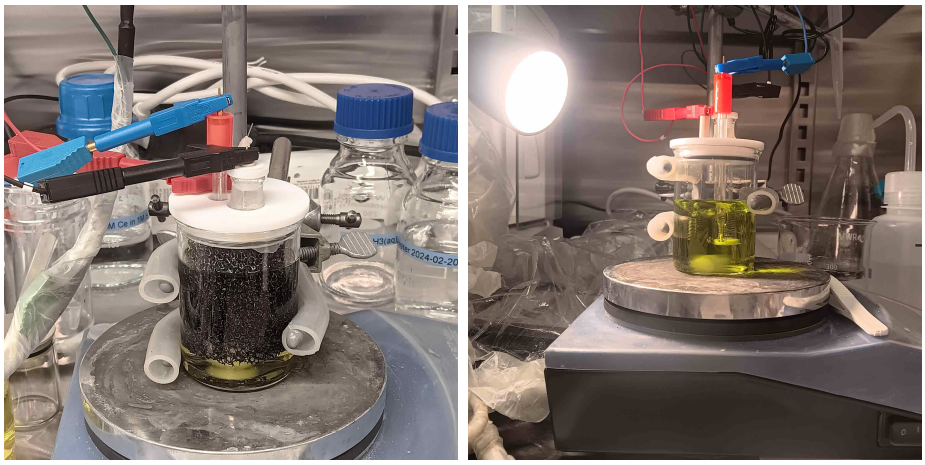

Figure 3.1: Electrochemical setup with glassy carbon working electrode (left) and platinum working electrode (right)

Different applied potentials were tested to see how they affected reduction speed, and the final general procedure ended up as: start a new batch with -0.45 V vs SCE for ca. 3 h, change to -0.6 V for ca. 6 h and then change again to a final potential of -0.65 V for ca. 8 h. Figure 3.2 shows the exact reducing potential applied over time for each batch.

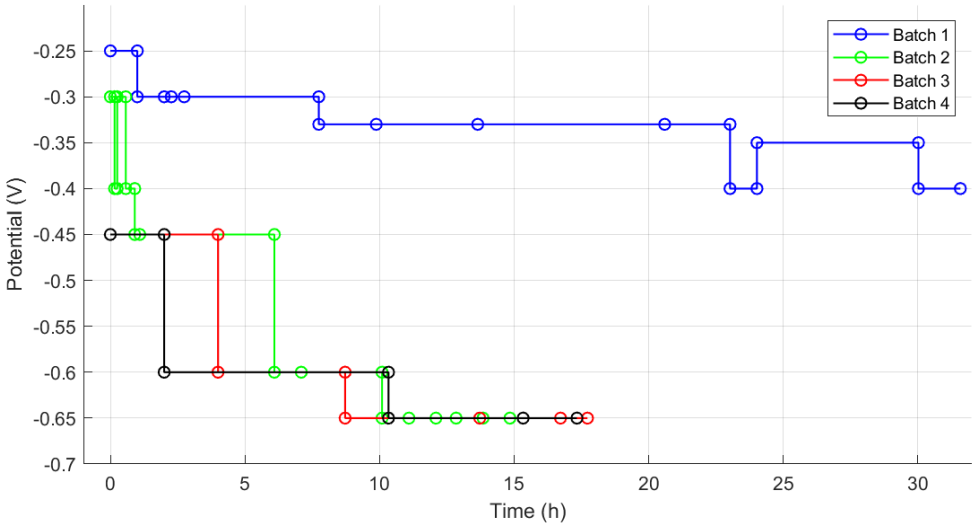

Figure 3.2: Graph showing the exact runtime with corresponding applied potential for all NP batches. Circles indicate independent run segments.

The 4 batches reduced had three different amounts of doping. Batch 1 had ca. 70 ml of U(VI) stock solution. An unknown amount of batch 1 was also thrown away when doing UV-Vis. Batch 2 was also 100% UO_2 and consisted of 65 ml of U(IV) stock solution, although an unknown but likely smaller amount was removed when testing different electrodes. Batch 3 was doped with 1 mol% Ce and 1 mol% La and 98 mol% U, ignoring the oxygen in the final powder/pellet. It consisted of 1.93 ml or 2.0254 g Ce stock solution, 1.54 ml or 1.5550 g La stock solution and 68.07

ml or 71.5094 g U stock solution. Total volume was 71.54 ml. The lanthanum was added after the electrochemical reduction. Batch 4 was doped with 5 % Ce and 1% La, and consisted of 9.95 ml or 10.6399 g Ce stock solution, 1.56 ml or 1.5810 g La stock solution and 68.53 ml or 72.29 g U stock solution. Total volume was 80.04 ml. The reported volumes of stock solution for B3 and B4 was the amount taken with a micropipette, which was then weighed on a scale which are the reported masses.

3.1.2.3 UV-Vis spectroscopy

UV-Vis spectroscopy was used to determine state of reduction. Since the total concentration of uranium is relatively high, it is impossible to use UV-Vis to determine concentration of U(IV) when the uranium is almost fully reduced, without diluting the UV-Vis sample. Therefor in order to avoid diluting the samples, the U(VI) peaks in the spectra were instead used, and when their values were negligible compared to the U(IV) peaks the reduction was deemed complete.

A VWR UV-6300PC Double Beam Spectrophotometer was used for the UV-Vis spectroscopy. A sample of the uranium solution was added to a UV-Vis vial with screw on lid to prevent oxidation of sample. An identical vial with pure 1 M $HClO_4$(aq) was used as reference. The instrument scanned wavelengths 700 nm to 350 nm with a step size of 0.2 nm, and an instrument setting called "precision" was set to 10 which corresponds to a scan speed of ca. 5.4 nm/s. The uranium sample was then brought back into the glovebox and added back to the bulk electrolysis solution.

3.1.2.4 Precipitation

After full reduction the uranium was precipitated using 0.5 M and 1 M NH_3(aq). The solution was transferred to a 250 ml glass bottle. A VWR pH 1100 L pH meter was used to measure the pH of the solution. The solution was stirred at between 500 to 800 rpm, increasing stir speed as the volume increased. The NH_3(aq) was added drop by drop so as to increase the pH slowly. For batch 1, 2 and partially 3 the NH_3(aq) was added by hand using two different 1 ml transfer pipettes, and therefor the total amount of NH_3(aq) or speed of addition was not properly recorded. For batch 4 and partially batch 3 the NH_3(aq) was added using a burette. 1 M NH_3(aq) was generally used in pH ranges where the pH increased little per drop, and 0.5 M NH_3(aq) was used when the ph increased rapidly.

The pH was brought up from 0 to between 1-2 in ca. 1.5 h, and was then left to sit for a few hours to a few days. More NH_3(aq) was added over ca. 30 min to a final pH of 8.5. Table 3.1 shows the pH values for each batch after the first addition of NH_3(aq), where the pH meter was not calibrated for B1 so the real pH value is unknown. It also shows the pH values after reaching equilibrium, as well as the final pH of the liquids.

Table 3.1: Table showing the ph values for each batch directly after the first addition of NH_3(aq), after reaching equilibrium (pH stops decreasing), and after the second/final addition.

Batch	**pH after first addition**	**pH after equilibrium**	**pH after final addition**
B1	n/a	0.75	8.51
B2	1.7	1.48	8.60
B3	1.5	0.99	8.50
B4	1.93	1.66	8.54

Table 3.2 shows the exact amount of NH_3(aq) added, speed of addition and the ph values after each addition. The last two additions were performed four days later when the solution had equilibrated, hence the big jump in pH. To precipitate batch 4 an equivalent total volume of ca. 84.5 ml 1 M NH_3(aq) was used.

Table 3.2: Table showing the precipitation of batch 4, with the equivalent amount of 1 M NH_3, the corresponding drop rate and pH levels after each addition of NH_3.

1 M NH_3(aq) equivalent [ml]	**Average drop rate [ml/min]**	**pH before**	**pH after**
10	0.53	-0.039	0.166
25	1.39	0.166	0.759
12.5	1.04	0.759	1.310
10	1,00	1.310	1.597
10	1.11	1.597	1.928
10	0.83	1.664	7.42
7	0.58	7.37	8.576

3.1.2.5 Filtering and drying

The precipitate suspension was filtered on a Cytiva 0.2 µm nylon membrane filter paper to separate the liquid from the particles, using a standard vacuum filtering setup with a vacuum pump located outside the glovebox. Two filtrations were carried out per batch as there were too many particles to filter everything in one go. The particles were washed with MQ water two times. The particles were put inside two plastic beakers, spread out as much as possible to increase surface area and put inside a desiccator with silica gel for drying. They were kept inside the desiccator until the next batch of particles were ready, which was around one week. However, drying in the glovebox without a desiccator appeared to take about as long time.

The procedure to connect and disconnect the vacuum pump without letting oxygen into the glovebox was as follows: connect vacuum hose to Büchner flask, unscrew cap nut on the outside of the glovebox, connect pump to glovebox, turn on pump, filter and wash the particles, disconnect hose from Büchner flask, hold hose in the air so as to not suck out any particles, disconnect pump from glovebox, screw on cap nut, cap the hose end inside the glovebox with finger, turn off pump, and pump out air inside hose using glovebox airlock intake.

3.1.2.6 Powder grinding and pellet pressing

After drying, ca. 0.9 g of the aggregated particles were ground into a fine powder using a mortar and pestle. Table 3.3 shows the amount of particles used for each pellet before grinding, together with powder/pellet dopant concentration. The mortar was placed on a clean piece of paper, and an ad hoc paper cylinder made from taped together paper tissues was placed around the mortar to catch particles escaping during grinding, so that they could be added back into the mortar.

Table 3.3: NM pellet powder masses before grinding, and nominal pellet dopant concentrations.

Pellet	**Powder mass [g]**	**at% La**	**at% Ce**
B1	0.9043	0	0
B2	0.9150	0	0
B3	0.9808	1	1
B4	0.9357	1	5

The powder was added into a 9 mm wolfram carbide pressing die. The die, together with a metal cylinder used to help press out the pellet from the die, was sealed in two plastic bags before being brought out of the glovebox. The pressing die was kept inside the bags during the whole pressing to keep an inert atmosphere. The pellet was pressed at a force of 1.5 tons which, using Equation 3.1, equals 232 MPa. The applied force decreased over time and needed to be continuously brought back up to 1.5 tons for the 30 minutes it took for the pellet particles to settle. The pressed pellets were stored in the glovebox until all were ready for sintering.

$$Pressure = \frac{m \cdot g}{r^2 \cdot \pi} \tag{3.1}$$

Were m is the mass 'force' applied by the press, g is the gravitational acceleration and r is the die radius.

3.1.2.7 Sintering

An Entech ETF 30-50/18 tube furnace was used for sintering, using an alumina tube and crucible. During sintering a 1 l/min 5%H_2, 95%Ar gas flow was applied. All seven pellets were sintered together three times at 1200 °C, 1650 °C and 1750 °C. The three temperature profiles are shown in Figure 3.3. After sintering the pellets were weighed and measured using a caliper to calculate their densities. When sintered the pellets were stable enough to be stored and handled outside the glovebox.

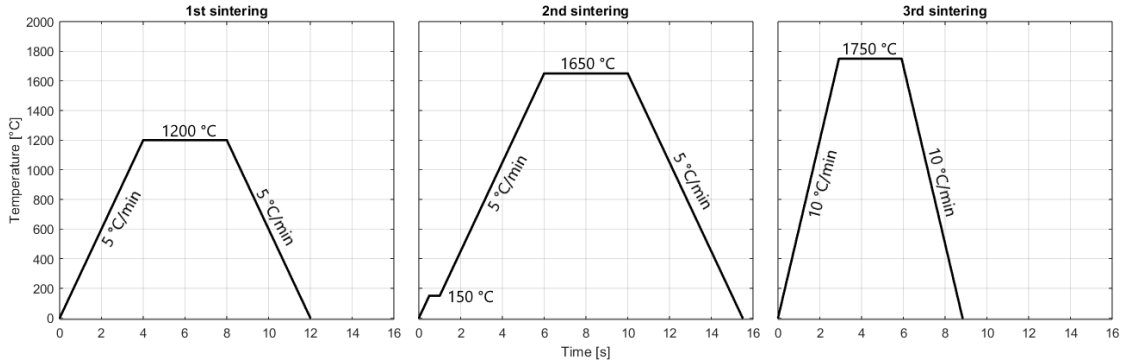

Figure 3.3: Temperature profiles for the 3 sintering steps. First sintering was kept at 1200 °C for 4 h. Second sintering was kept at 150 °C for 30 min and 1650 °C for 4 h. Third sintering was kept at 1750 °C for 3 h.

3.1.3 Reference pellets

Three UO_2 reference pellets were made with no dopants, 1% Ce and 5% Ce, using a method which is sometimes (erroneously) called the ADU process. No part of the reference pellet synthesis was conducted inside the glovebox.

0.9604 g and 5.0212 g of a 0.084 M Ce nitric acid solution was added to two vials, to make the 1% and 5% Ce doped UO_2. 4 ml 2.09 M uranyl nitrate was added to each vial. The contents were poured into two separate centrifuge vials containing small stir bars, and was stirred on a stir plate. Over 10 ml NH_3(aq) was added to each vial to precipitate the uranium and cerium. The vials were centrifuged at 4000 rpm for 5 min. The ammonium was decanted and ethanol was added to dissolve the solid substance. The ethanol and doped uranium was added into separate plastic beakers and left to dry. The undoped UO_2 was made by simple adding NH_3(aq) to 4 ml 2.09 M uranyl nitrate and left to dry.

Almost two months later the dry powders were reduced in a tube furnace. The powders do not require anywhere near two months to dry. The powders were added into 3 separate alumina crucibles and the stir bars were removed before the crucibles were put int the furnace. The temperature profile was 0 °C to 200 °C, 3 °C/min, to 1200 °C, 10 °C/min, hold 3 h, back down to 0 °C, 10°C/min. A 5% H_2, 95% Ar gas with flow rate of 1 l/min was applied inside the tube.

The reduced powders were ground by hand with mortar and pestle into a fine powder, which was thoroughly cleaned with ethanol between each powder. The powders were pressed into pellets with an applied force of 1.5 ton. They were then sintered together with the NM pellets. The amount of ground powder used for each pellet, together with pellet dopant concentrations, is shows in Table 3.4.

Table 3.4: Reference pellet powder masses before sintering, and nominal pellet dopant concentrations.

Pellet	Powder mass [g]	at% Ce
R1	0.9324	0
R2	0.9077	1
R3	0.8963	5

3.2 Characterisation

All of the following methods were conducted outside the glovebox in normal atmosphere.

3.2.1 ICP-MS

A Thermo Scientific iCAP Q ICP-MS was used on stock solutions and uranium powders to ascertain their elemental composition. All measurements used 0, 1, 5, 10, 25, 50 and 100 ppb standards for the respective elements, with 1 ppb Bi internal standard. To measure the powders a small amount from what was left after making pellets was taken, weighed and dissolved in strong nitric acid (HNO_3(aq)). Then the solutions were diluted two times so that the concentration of analyte in the final solution should lie close to 1-100 ppb. The standards were measured to later create a line equation relating counts per minute to concentration in ppb. Excel was used to analyze the data. For the stock solutions the concentration of the origin solution was calculated, while for the powders only the relative quantity of U, Ce and La after being dissolved was needed to get the atomic percentages in the powders.

3.2.2 Pycnometry

A micromeritics AccuPyc II 1340 Gas Pycnometer using helium gas was used to measure the volume of each pellet. This instrument is blind to open porosity so the measured volume excludes the volume of open pores in the sample. This volume was then used to calculate a more accurate density for each pellet. Before measuring of the pellet volume a steel ball with a known volume was measured to later calibrate the measured volumes with regards to the pycnometers deviance. Since the pellets were too small to get accurate measurements a small screw with a measured volume was added together with each pellet and the screw volume was subtracted from the total volume to get the pellet volume.

3.2.3 PXRD

X-ray diffractograms for all pellets were taken using a Bruker D2 Phaser Tabletop Powder X-ray Analyzer. The sintered pellets were broken into 2-4 pieces using a flathead screwdriver and rubber mallet. The largest pieces were kept to later be used for Light Optical Spectroscopy (LOM) and SEM. One or two smaller pieces

of each pellet were ground down into a fine powder using a pestle and mortar, the equipment cleaned thoroughly with ethanol between each use.

The powders were taken into the glovebox where the instrument was kept and added onto a zero background holder. The powder was flattened using the short side of a glass pane to avoid selective alignment of crystal facets.

The data was analyzed using the DIFFRAC.EVA software and compared to a database of x-ray diffraction results to ascertain unit cell and estimate lattice parameter. This is to see that the powders have the UO_2 crystal structure and how the doping affects the lattice parameter.

3.2.4 Pellet grinding and polishing

All pellets were first polished by hand but this gave unsatisfactory results when viewing the pellets in the LOM.

To get better results from LOM and SEM the pellets were grinded and polished using a Struers LaboForce-50 polishing instrument. To use this instrument the pellets were first encased in larger epoxy pellets, which is necessary for them to fit in the instrument, prevents them from breaking apart during grinding and helps prevent pieces of the pellets from contaminating the LOM and SEM instruments. All 7 pellets were encased in 4 pellets, with B1 being alone and the other NM pellets paired with their respective reference pellets. The epoxy was made with 5:1 g resin to hardener and left to harden over two days.

For the entire polishing the rotational speed was kept below 100 rpm, with a lower pressing force. Struers silicon carbide sandpapers were used first, followed suspension polishing. The sandpaper grits used in order were: 220, 500, 800, 1000, 1200, 2000 and 4000, in the FEPA-P scale. MQ water was used as lubricant and added so that the papers always had a layer of water on them. After the 4000 grit sandpaper a Struers DiaPro Dur 3 µm diamond suspension on a MD-Dur soft paper was used, followed by DiaPro Nap B 1 µm diamond suspension on MD-Nap. The final polishing used OP-S NonDry colloidal silica suspension on MD-Chem. The coarser sandpapers were used for only a few minutes until the paper was visible covered in a layer of brown UO_2 powder. The finer sandpapers that did not remove enough material to be visible on the paper was used for longer and the pellets were inspected until they were noticeably smoother. The suspension polishes were used for the longest, up to 30 min. Between the 1200, 2000 and 4000 grit papers the pellets were cleaned with ethanol using paper tissues. Between the suspension polishes and after the final silica polish, the pellets were cleaned in ethanol in an ultrasonic bath for 5 minutes to remove suspension particles. The epoxy pellet holder was also cleaned with ethanol when changing suspension.

3.2.5 LOM

A Zeiss Axio Vert.A1 LOM was used to visually examine the polished pellet surfaces. The LOM was used to determine success of polishing, see if there were any visible dopant aggregates, look at pellet porosity and possibly see grain sizes. The zoom

levels available were 5x, 10x, 20x, 50x and 100x.

3.2.6 Pellet etching

Pellet B1 was etched after polishing and initial LOM inspection. The etching solution was made from 10 ml of 12 M H_2SO_4 and 10 ml of 10 M H_2O_2. A drop of the solution was added onto the pellet surface for 10-15 s and then washed away with MQ water. Between each etching the pellet was inspected with the LOM. The pellet was etched four times with durations of 10 s, 10 s, 15 s and 10 s each, with a total time of 45 s. For the first etching the solution was still warm from mixing.

3.2.7 SEM and EDX

A FEI Quanta 200 ESEM FEG scanning electron microscope was used to analyze pellets B1, B3, B4, R2 and R3. It was operated at high vacuum with a voltage of 10 kV and a spot size of 3. The epoxy encased samples were mounted on a holder using carbon tape, with copper tape connecting the uranium pellets to the electrically conducting holder. Secondary electron, backscattered electron and something called Mix mode were all used to look at the samples. BSE was used primarily to look at grain structure.

EDX was also performed concurrently, using the AZtec software, to estimate homogeneity of the dopants in the pellets. EDX line scans were used primarily, but point analyzes and EDX mappings were also made on some samples. The most amount of line scans, six and four, were performed on pellets B4 and B3 respectively, as these were of most interest to analyze homogeneity.

4

Results and Discussion

4.1 Reduction of uranium

The method for electrochemical reduction of U(VI) to U(IV) was improved along the course of the project. Batch 1 was reduced using the glassy carbon WE. This electrode had a few drawbacks which included: being so large that only a 10 mm stir bar could be used, limiting stirring of the liquid and in turn possibly limiting reduction rate; the volume of the WE itself could possibly limit stirring; it was difficult to remove all solution stuck inside the large pores; small pieces could easily break off; and it prevented being able to see the CE and RE inside. Therefor a Pt WE was also tested and compared to the glassy carbon electrode. At an applied potential of -0.3 V the Pt electrode was better by around 1000 µA, while at a potential of -0.4 V the electrodes performed similarly. The Pt electrode had marginally higher current, meaning higher rate of reduction, but more importantly was easier to work with and was therefor chosen over the glassy carbon for the 3 other batches.

The maximum applied potential increased in magnitude over the course of the project, from -0.3 V to -0.65 V. With a higher potential the total reduction time decreased, as is shown in Figure 3.2, from above 31 h to below 18 h. Batch 3 and 4 took just over 17 h while batch 2 only took 14 h 50 min, and they all have a similar final U(VI) UV-Vis peak. Batch 2 did have slightly less U stock solution which would decrease time of reduction, but it is more likely that batch 3 and 4 was reduced longer than necessary, as the number of UV-Vis scans done on them was much less frequent. A potential even lower than -0.65 V was never tried mainly because the battery of potentiostat was starting to become a limiting factor in how fast a batch of U(VI) could be reduced. For future studies even higher in magnitude potentials could be tried to lower reduction time further, using a better potentiostat.

4.2 Sintering and density

After the first sintering the NM pellets had visibly shrunk while the reference pellets appeared to still be the same size. The NM pellets had cracked a lot, especially pellet B1 which had lost a lot of pieces that had flaked off. B1 looked akin to a rose on one side while the other side was uncracked. B2 and B3 had cracked in more typical manners, while B4 had only a few barely visible cracks. Pellets B2, B3 and B4 are shown in Figure 4.1 where, including the cracks, it can also be seen how the doping changes the color of the pellet from a dark brown to more black.

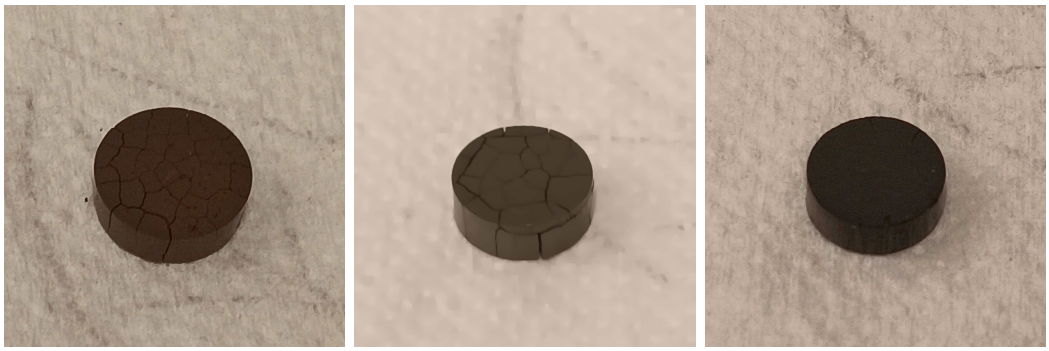

Figure 4.1: Pellets B2-B4, from left to right, after first sintering.

The pellet masses and densities after each sintering step are shown in Table 4.1. As it was assumed a caliper could give inaccurate results or possible damage unsintered pellets no measurements were taken before sintering or on the reference pellets after the first sintering. B1's dimensions were not measured as the uneven surface wouldn't yield any good results, and doing so might have caused more material to flake off.

Table 4.1: All pellet densities after each of the three sintering steps as measured by scale and caliper. TD_{UO_2}=10.96 g/cm3. All pellet volumes and masses can be seen in Table A.1.

Pellet	**B1**	**B2**	**B3**	**B4**	**R1**	**R2**	**R3**
Mass before pressing [g]	0.9043	0.9150	0.9808	0.9357	0.9324	0.9077	0.8963
Mass after pressing [g]	0.8861	0.8857	0.9434	0.9008	n/a	n/a	n/a
Mass after 1st sintering [g]	0.6994	0.8087	0.8654	0.8270	0.8451	0.9038	0.8930
Density after 1st sintering [g/cm3]	n/a	7.22	6.74	8.29	n/a	n/a	n/a
TD_{UO_2} [%]	n/a	65.9	61.5	75.7	n/a	n/a	n/a
Density after 2nd sintering [g/cm3]	n/a	9.51	10.29	9.76	6.91	8.74	9.83
TD_{UO_2} [%]	n/a	86.7	93.9	89.1	63.1	79.8	89.7
Density after 3rd sintering [g/cm3]	n/a	9.65	10.19	9.55	7.02	8.97	9.95
TD_{UO_2} [%]	n/a	88.1	93.0	87.1	64.1	81.9	90.8

After the second sintering step the cracks in B2 and B3 were still visible but had closed up significantly, while the circular cracks of B1 remained. All NM pellets shrank further, which could be discerned with the naked eye and the difference in volume is reflected in the change in density as shown in Table 4.1. After the first sintering did the mass of the NM pellets decrease with an average of 8.4%, not counting B1 because of the flaking after sintering. The mass of reference pellets R2

and R3 decreased with only 0.4%, not counting R1 since it was not weighed again after being damaged before sintering. The significant difference in mass change between the NM and reference pellets is likely due to the NM pellets not being fully dry, while the reference pellets had an insignificant amount of bound water since they had a smaller surface area and, more importantly, had already been heated in the furnace once before. A more detailed table with pellet masses and volumes after each sintering can be found in Table A.1 in the appendix.

The mass of all pellets did not change much after the second and third sintering. The reference pellets visually appeared to have shrunk during the second sintering. The calculated density of the NM pellets increased significantly, but all pellets, except R1, remain at only around 90% of the theoretical density for UO_2, using a caliper to measure the volume.

Figure 4.2 show all pellets before and after the third sintering, showing that there was little visible difference caused by the third sintering. At the top is visible all the material that flaked off pellet B1. The images also show the visible size difference between the NM pellets and reference pellets. The surface of pellet B4 only looks different between the images because it was flipped over.

Figure 4.2: All seven pellets (from top to bottom: B1-B4, R1-R3) after the second sintering (left) and after the third sintering (right).

Pellet R1 was damaged before the first sintering and no longer had a circular shape, so therefor the reported volumes and densities are not accurate. However the mass of pellets R2 and R3 did not change much after sintering, so the R1 mass before pressing, 0.9324 g, can be used instead to calculate an approximate final density of 7.76 g/cm3. This density is still low compared to the other pellets, which could indicate that it is rather porous, possibly caused by the mentioned damage, or maybe poor powder grinding before pressing.

After the third sintering the density went up a small amount for B2 and the reference pellets, while for B3 and B4 the density decreased by a small amount. The changes in densities is only between 0.1-0.2 g/cm3. The mass change is low and could likely be inaccuracy from the scale. The volume change is no larger than 0.002 cm3 for

any pellet, which could also possibly be explained by variation in measurement with the caliper, especially considering that most pellets were shaped more like truncated cones rather than perfect cylinders. It is worth noting that the doped pellets could never achieve 100% TD_{UO_2} as the Ce and La, being lighter elements, will lower the pellets' maximum theoretical density.

The so called rose structure of pellet B1 after the third sintering can be seen in Figure 4.3.

Figure 4.3: The "underside" of pellet B1 after sintering three times.

4.2.1 Pycnometry

The volume obtained from pycnometry for each pellet is presented in Table 4.2 together with calculated density and percentage of theoretical UO_2 density. That B4 and R3 have lower densities than the others is to be expected as they contain the most amount of dopants, while B2 having such a relatively low density despite having no dopants could be because of higher closed porosity inside the pellet. The densities are higher for all pellets compared to the geometrically calculated densities in Table 4.1. This means that all pellets contain open pores, with the percentage of open porosity shown in Table 4.3. There is a possible trend of Ce doping decreasing open porosity but the number of pellets is too low to come to any certain conclusion. The average open porosity of the NPs and the reference pellets are 7,57% and 17,7% respectively. This points to the NM pellet synthesis route making more dense pellets compared to the more standard ADU process.

Table 4.2: Pellet volumes and densities obtained from helium pycnometry measurements. TD_{UO_2}=10.96 g/cm3.

Pellets	**B1**	**B2**	**B3**	**B4**	**R1**	**R2**	**R3**
Volume [cm3]	0,0654	0,0738	0,0809	0,0804	0,0782	0,0847	0,0876
Density [g/cm3]	10,67	10,29	10,66	10,23	10,78	10,65	10,15
TD_{UO_2} [%]	97,35	93,93	97,27	93,36	98,40	97,15	92,64

Table 4.3: Amount of open porosity calculated from caliper measured volume and pycnometry obtained volume.

Pellet	**B1**	**B2**	**B3**	**B4**	**R1**	**R2**	**R3**
Open porosity [%]	n/a	11,7	4,37	6,62	34,8	16,1	2,10

4.3 ICP-MS data

4.3.1 Stock solutions

Table 4.4 shows the concentrations of U, Ce and La in the respective stock solutions as measured with ICP-MS. They all had lower concentration then the one intended when made. For the uranium it might be that the initial precipitate was not centrifuged enough during making. For the cerium and lanthanum solutions it is suspected that their respective nitrate hexahydrate sources have absorbed more water over time in storage.

Table 4.4: Concentrations of the 3 stock solutions measured with ICP-MS, together with the wanted concentrations.

Solution	U	Ce	La
Concentration ICP [mM]	91.91	33.68	42.62
Target Concentration [mM]	100	50	50

4.3.2 UO_2 powders

The ICP-MS derived elemental composition of the 4 NM powders, before pressing and sintering, is shown in Table 4.5. The undoped B1 and B2 have next to no La or Ce as expected. The negative La amounts come from the fact that fitting curves to the standards can sometimes give a negative constant in the linear equation, which gives negative amounts for really small input values. This can be circumnavigated by forcing the line through the origin but that is often frowned upon. The amount of La in B3 and B4 are really close to the desired 1%, while the amount of doped cerium is higher than the expected values of 1% and 5% for B3 and B4. The amount of Ce is 50% and 44% higher, respectively, than expected. The reason for this could have been that too much was erroneously added during the synthesis. But since the error is similar for both powders, it is also likely that it is the Ce stock solution which has a higher concentration than what was measured with ICP-MS. Either way these Ce concentrations are still within a reasonable interval to serve their purpose in this project.

The Ce doping in the reference pellets, also shown in Table 4.5, is close to the desired 1% and 5%.

Table 4.5: Relative molar percentage of La, Ce and U in all synthesized powders as measured with ICP-MS.

Powders	**B1**	**B2**	**B3**	**B4**	**R1**	**R2**	**R3**
U [at%]	99,94	99,93	97,37	91,77	99,96	98,89	94,61
Ce [at%]	0,09	0,10	1,50	7,19	0,03	1,11	5,38
La [at%]	-0,03	-0,03	1,14	1,04	0,01	0,01	0,01

4.4 PXRD data

PXRD results for all pellets are shown in Figures 4.4 to 4.10. All diffractograms are unsurprisingly similar, except for B2. The amount of powder taken from B2 was not sufficient to make a smooth and even surface like the other powders. This has decreased overall peak height, changed relative peak heights, slightly broadened the peaks, and increased noise. In all Figures except 4.5 and 4.7 there is a smaller peak to the left of all main peaks. When the PXRD was performed most powders were arranged in flat top peaks, together with non-flattened powder surrounding the peak. This more randomly strewn powder was likely the cause for the smaller peaks seen in the Figures.

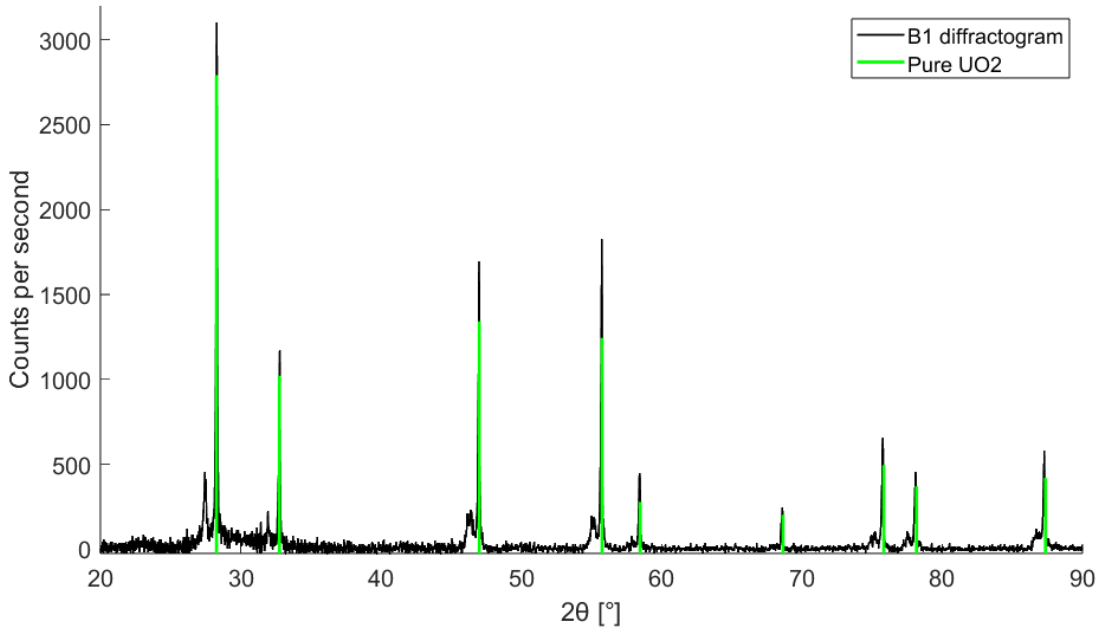

Figure 4.4: X-ray diffractogram of B1 and UO_2 reference.

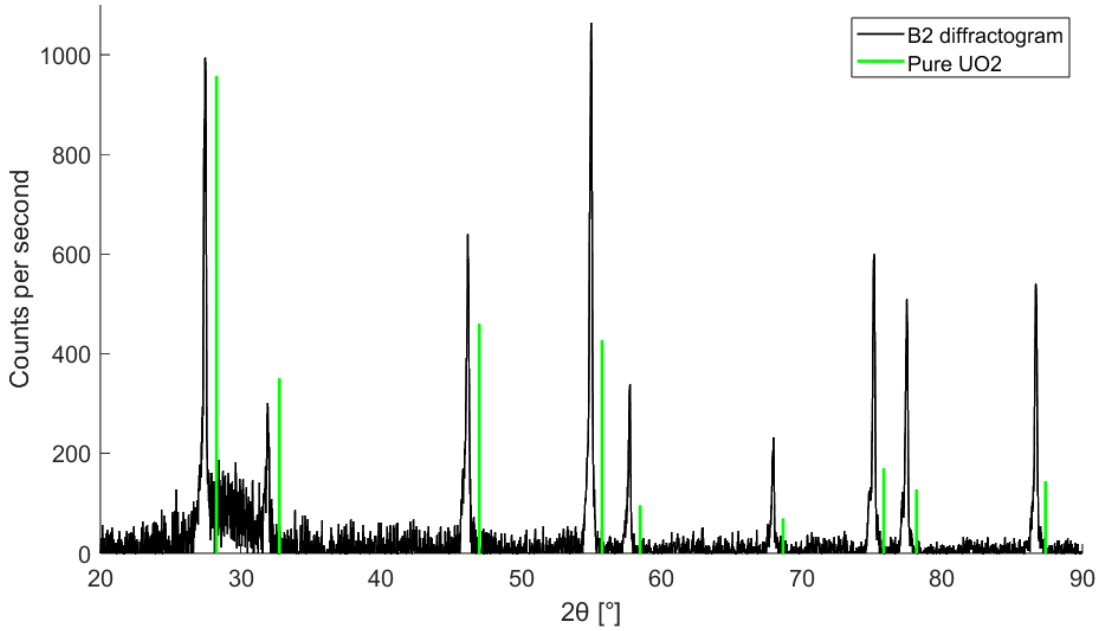

Figure 4.5: X-ray diffractogram of B2 and UO_2 reference.

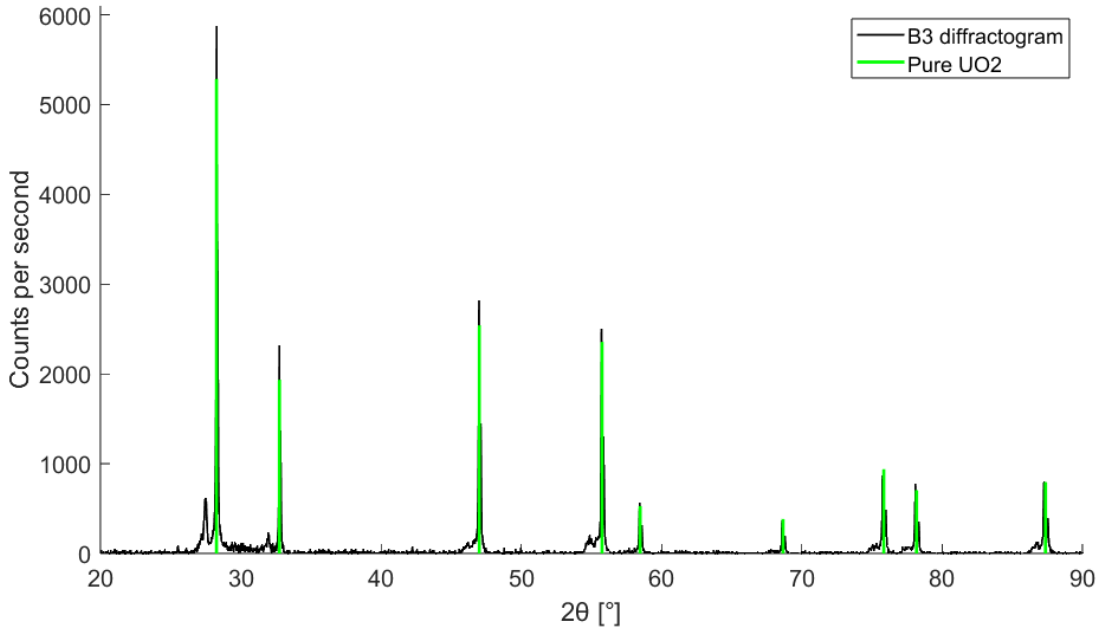

Figure 4.6: X-ray diffractogram of B3 and UO_2 reference.

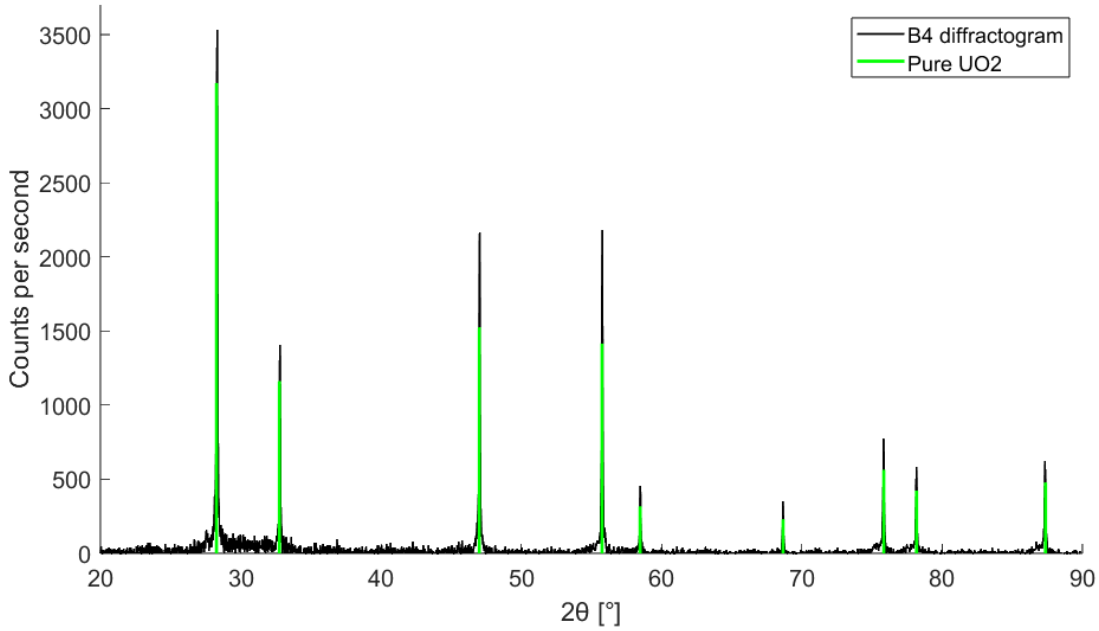

Figure 4.7: X-ray diffractogram of B4 and UO_2 reference.

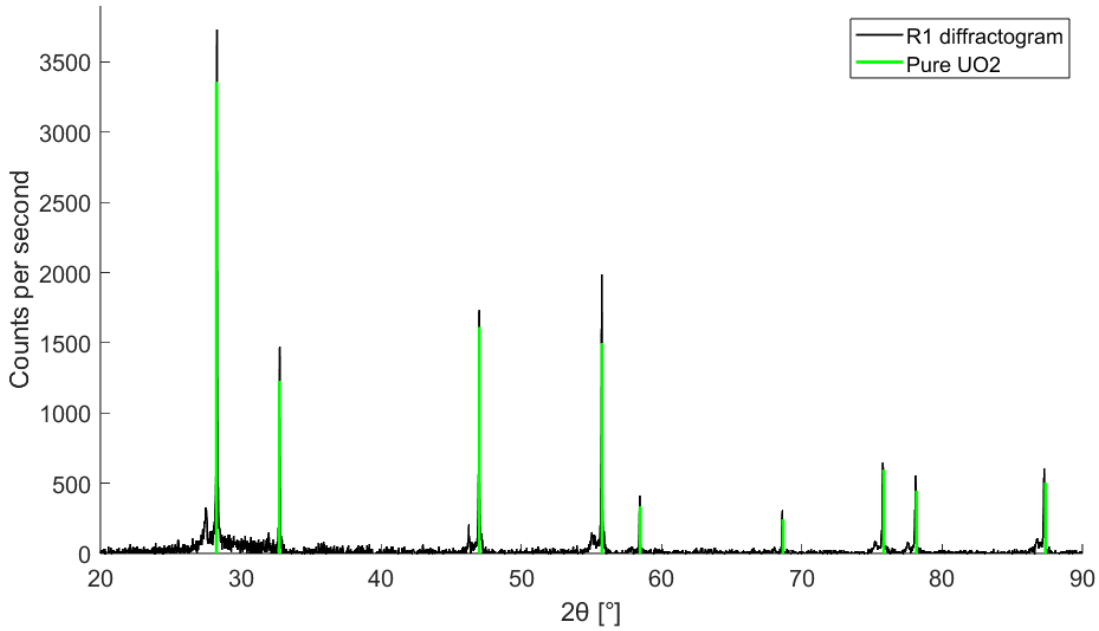

Figure 4.8: X-ray diffractogram of R1 and UO_2 reference.

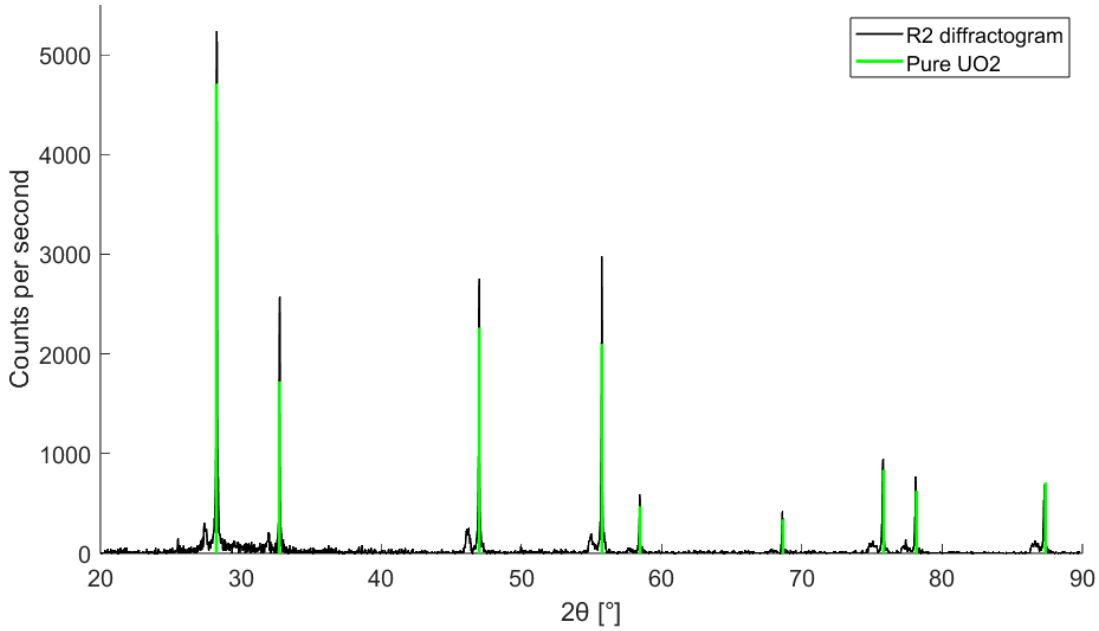

Figure 4.9: X-ray diffractogram of R2 and UO_2 reference.

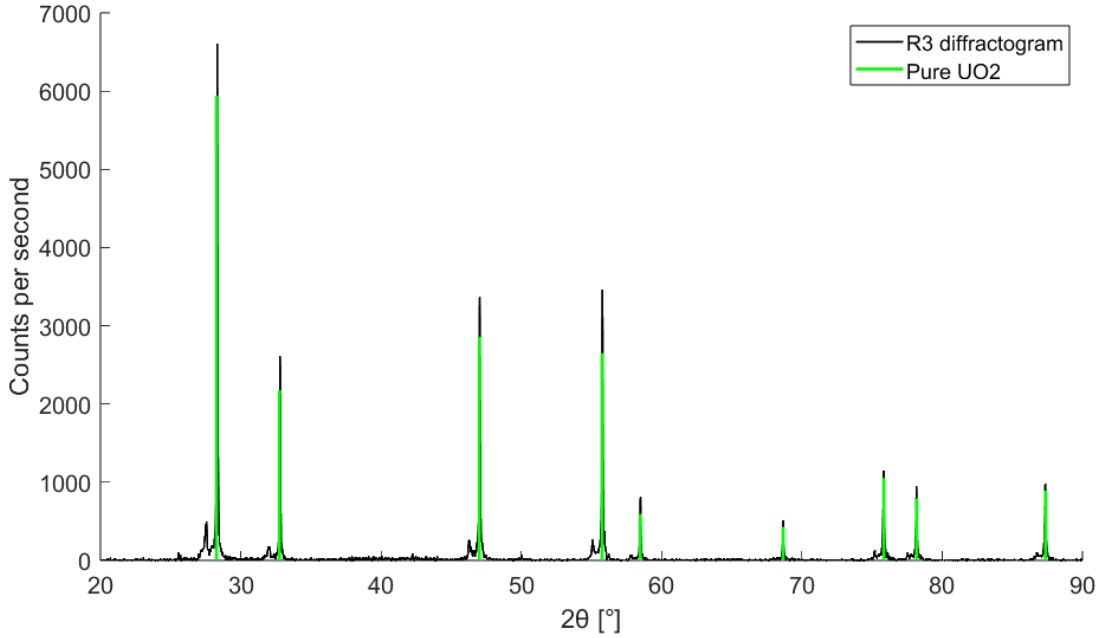

Figure 4.10: X-ray diffractogram of R3 and UO_2 reference.

A trend can be seen with both the NM and reference pellets; the peaks of the highly doped UO_2 are shifted slightly to the right compared to the undoped UO_2. This is most noticeable for the higher angle peaks, when compared to the green UO_2 reference peaks which are at the same angles in all diffractograms. This shift corresponds to a contraction of the unit cell with increasing dopant level. The best

lattice parameter match that could be found in the database for each pellet is shown in Table 4.6. These values are only the best match from a database, so they are not fully accurate. The table also shows lattice parameters calculated from the diffractogram peaks, which should be more accurate than the database parameters. Both methods show a similar trend of parameter increase from no dopant, B1, B2 and R1, to low dopant level, B3 and R2. But at the highest dopant level, B4 and R3, the parameter is smaller than the undoped UO_2. This data implies that a small amount of Ce and/or La doping will increase the lattice parameter, while a relatively larger amount will decrease the lattice parameter of the crystal structure. According to what is stated in the theory, the lattice parameter should only decrease with increased dopant level for the reference pellets, as they only have Ce. It is likely that the small increase from R1 to R2 is because of error in measurement. But if the data is correct, it might possibly be that the Ce(III) in R2 did not oxidise and increases the parameter similar to La(III). For the NM pellet, B3, it could be possible that the lattice parameter increase caused by the La is greater than the decrease caused by Ce.

Table 4.6: Lattice parameter for each pellet as decided by the best match in a crystallographic database, as well as lattice parameters calculated using Equations 2.6 and 2.7 with the nine 2θ peaks from each XRD graph. The calculated parameter for B2 is much smaller than the database parameter because of the poor diffractogram.

Pellets	**B1**	**B2**	**B3**	**B4**	**R1**	**R2**	**R3**
Database lattice parameter [Å]	5.4638	5.4638	5.4660	5.4590	5.4638	5.4651	5.4590
Calculated lattice parameter [Å]	5.4656	5.5402	5.4669	5.4616	5.4647	5.4652	5.4610

4.5 LOM imaging

The LOM was first used to look at the pellets after polishing by hand. The surfaces were deemed not sufficiently smooth and the pellets were encased in epoxy and polished more thoroughly by machine. After machine polishing the surfaces were smooth, as seen in Figure 4.11 showing the NM pellets, and Figure 4.12 showing the reference pellets. All images were taken at 100x magnification and are a combination of grayscale and full color. There is a noticeable correlation between the amount of pores on each pellet surface and their respective amount of open porosity shown in Table 4.3. Most striking is pellet R1 which has the highest open porosity of 34.8% and by far the most pores in the LOM images. Pellet B3 had the least amount of open porosity at 4.37% which also shows in its smooth surface in the LOM image. Of course these images are not fully representative of each pellet, but the pellets' porosity was rather homogeneous, with the occasional larger pores or cracks.

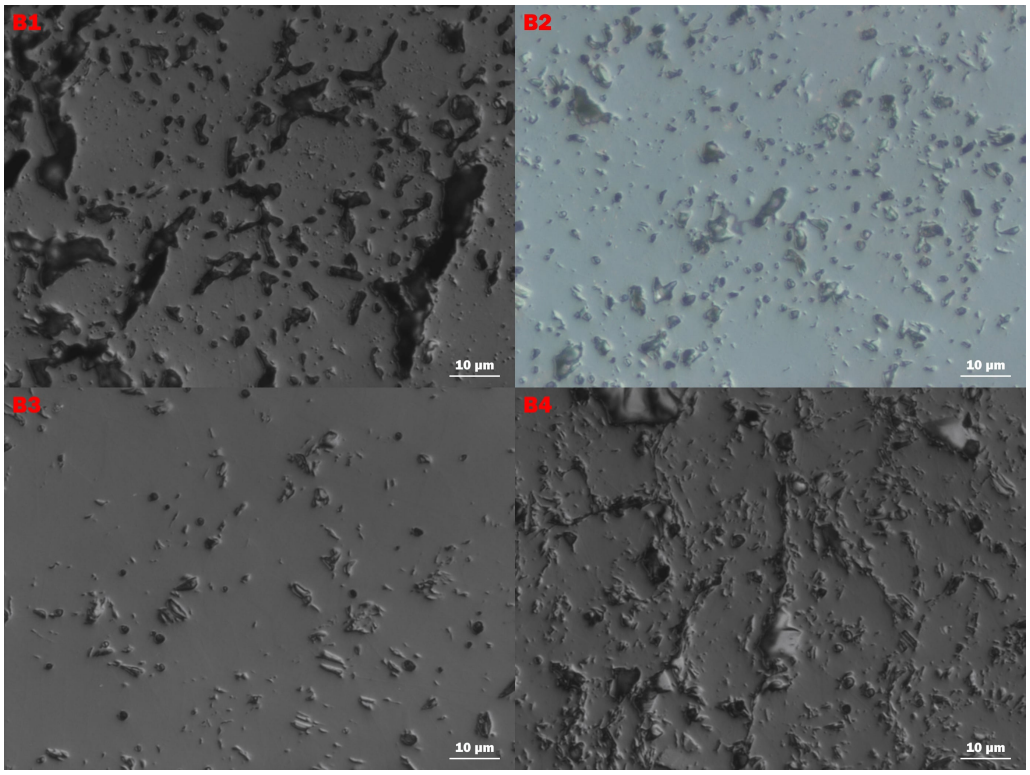

Figure 4.11: Images of polished NM pellets B1-4 at 100x magnification. The B1, B3 and B4 images were taken in grayscale while the B2 image is in color.

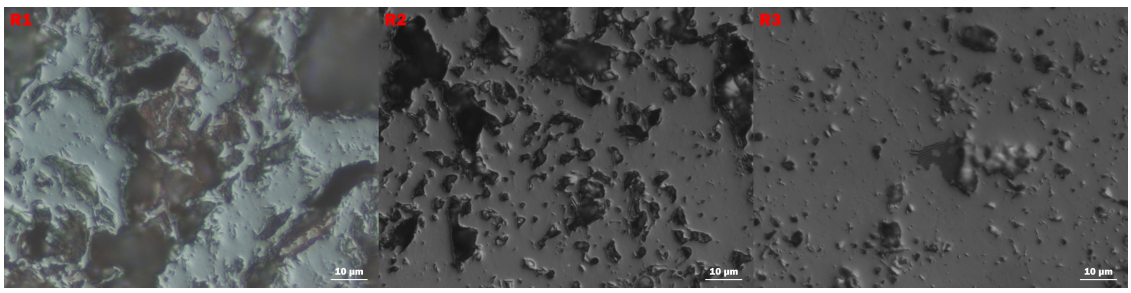

Figure 4.12: Images of polished reference pellets R1-3 at 100x magnification. The R2 and R3 images were taken in grayscale while the R1 image is in color.

Furthermore the LOM images shows that neither the NM pellets nor the reference pellets have any visible Ce or La aggregates, as such aggregates would likely show up as bright spots as shown in Helena Oliva's Master thesis[2]. Less zoomed in images with 5x magnification for pellets B1-4, shown in Figure 4.13, show that the pellets are homogeneous throughout the surface, barring cracks and occasional larger pores. The dark color in the cracks, especially noticeable in B2, is the epoxy.

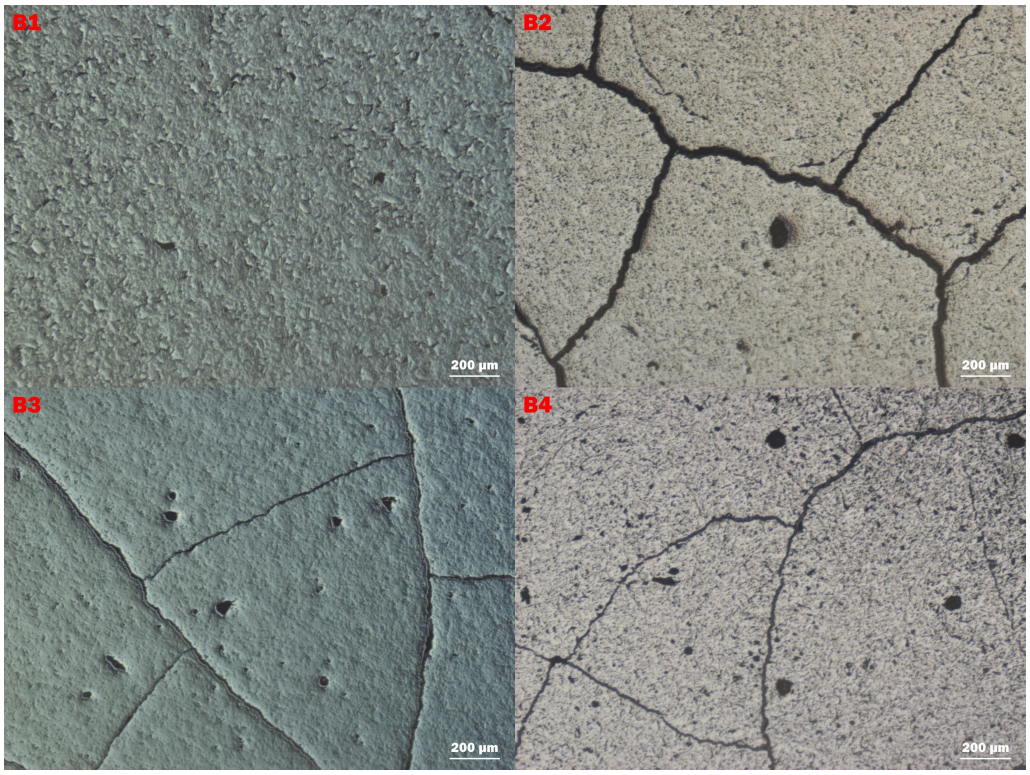

Figure 4.13: Images of polished NM pellets B1-4 at 5x magnification. The difference in color between the pellets come from the images being taken with different filters.

The LOM did not show any grain boundaries because of the polishing hiding them. Therefor etching was performed on pellet B1 to see if this would reveal any grain structure. Etching was only performed on pellet B1 as there was no precise method available to follow, meaning it was unknown how good the results would be or if the pellet would be etched too much. The acidic etching solution dissolve the boundaries between grains faster than the grains themselves, creating grooves visible in microscopy[26]. LOM images of B1 after a total of 45 s of etching is shown in Figure 4.14, showing that the etching was successful.

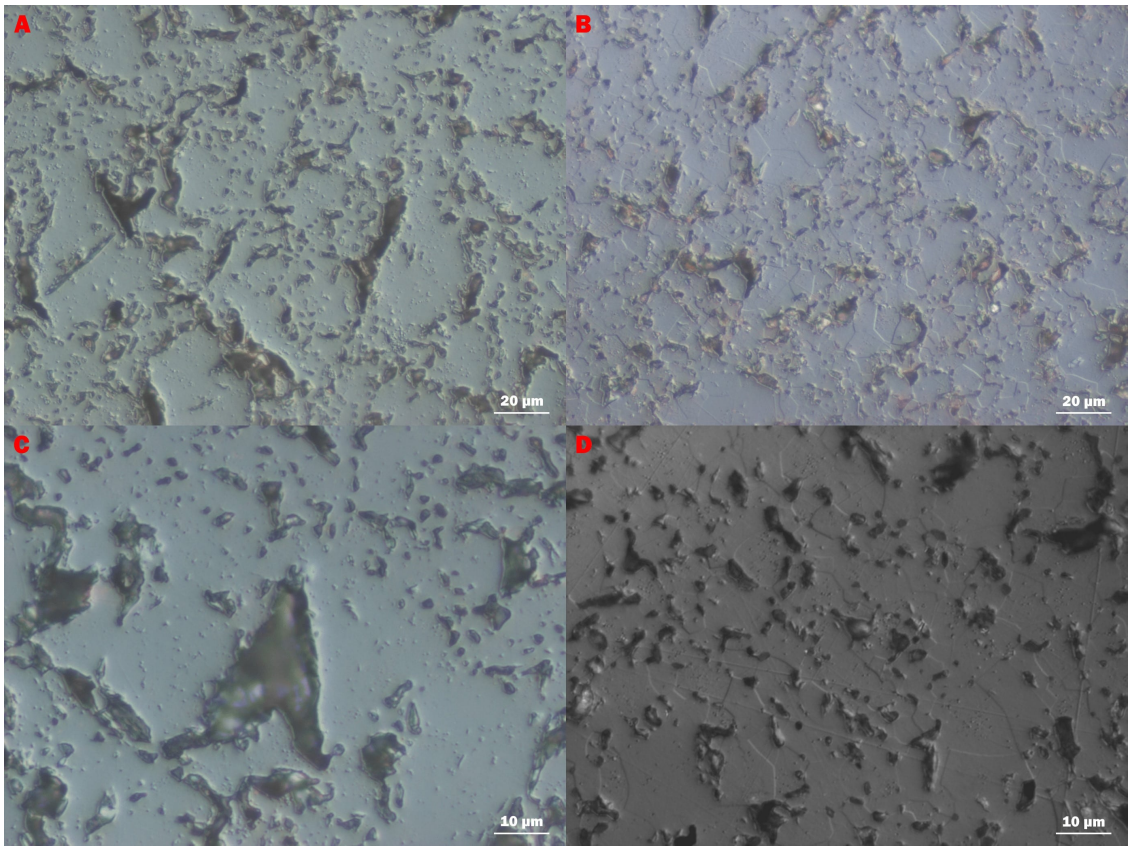

Figure 4.14: LOM images before (A) and after (B) 45 s etching at 50x magnification, and before (C) and after (D) etching at 100x magnification. Color differences are because the images were taken with different filters and/or in grayscale.

The long straight lines in Figure 4.14 B and D are presumably grooves from the polishing that have been made more visible because of the etching, while the shorter lines that form geometric shapes are the grain boundaries of the pellet. These grain boundaries are not visible in images A and C. The smallest visible grains in image D have a diameter of around 5 µm while the larger grains seem to be on the scale of 30-40 µm. Though, it is hard to tell where the exact boundaries of the largest grains lie. Either way the grains are larger than what was desired, but this is not unexpected. Behaviour of the NM pellets such as sintering at the relatively low temperature of 1200 °C confirms that the powders were nanometric, but the higher temperature sintering of 1650 and 1750 °C must have caused the grains to grow in size up to the micrometer scale.

4.6 SEM imaging

With the SEM it was easy distinguish between different different grains regardless of if the pellet had been etched or not. BSE were better at seeing different grains, but SE could also be used given the right settings. No dopant aggregates were spotted in the NM pellets nor reference pellets using SEM imaging. Figure 4.15 shows an image of pellet B1 where the different grains can be clearly differentiated. The grain in this image have sizes between roughly 3 µm up to 25 µm, although the smaller grains could be just the top of a grain, with their actual maximum diameter being larger. The grain size was measured as the longest straight length across a grain.

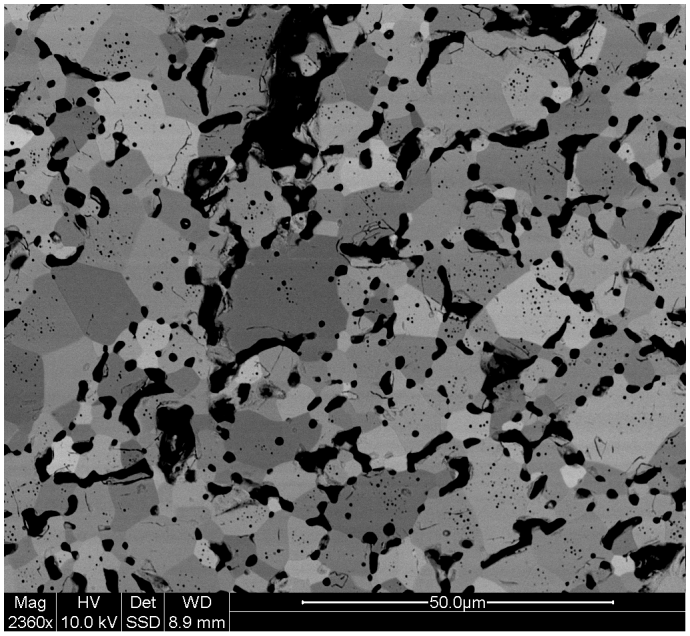

Figure 4.15: Backscattered electron SEM image of pellet B1. The differently shaded regions are different grains.

Figure 4.16 is a comparison between pellet B4 and its corresponding reference pellet R3. The R3 image has been resized to match its scale bar with that of the B4 image. It can be seen that the two pellets have similar grain sizes, with B4 having grains in the range of 4-15 µm and R3 3-17 µm.

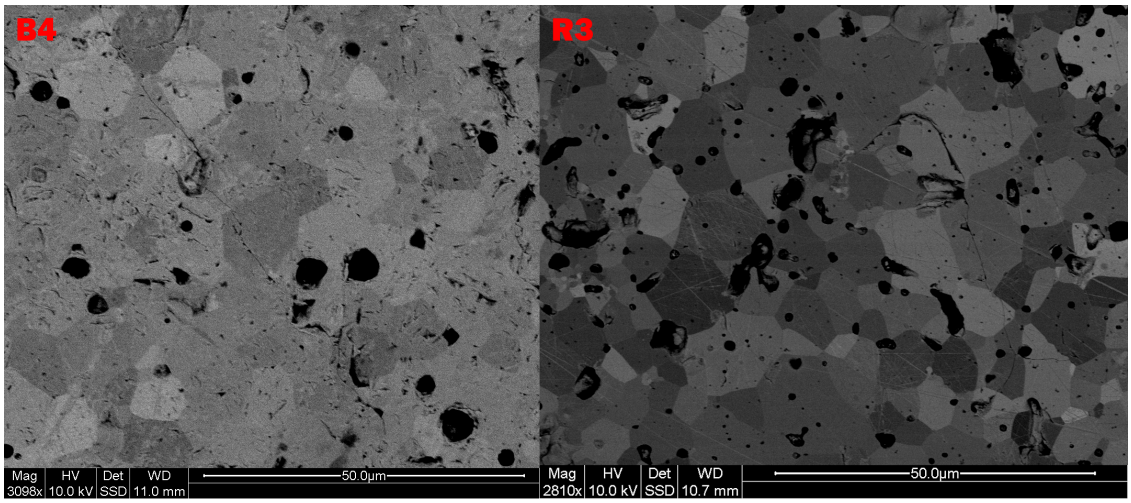

Figure 4.16: Backscattered electron SEM images of pellet B4 and R3. The R3 image has been resized to the same length scale as the B4 image.

The NM pellets were not completely homogeneous in their grain size distribution, as on both pellet B3 and B4 there were regions of smaller grain sizes, always together with increased porosity in the 3 regions found. Figure 4.17 shows two of these regions, and Figure 4.18 shows a zoomed in image of the region in Figure 4.17 B4. The grains in this image have size distribution of roughly 1.2-4 µm. It is a known phenomenon that pores can slow down grain growth during sintering[12], which is likely what has happened in the these cases.

Another possible cause could be inhomogeneity in the NP aggregate sizes before sintering. The NPs were found aggregated after drying and was therefor ground by hand to a finer powder before pellet pressing. The grinding likely created a size difference in aggregates that might have caused these regions of smaller grain sizes during sintering.

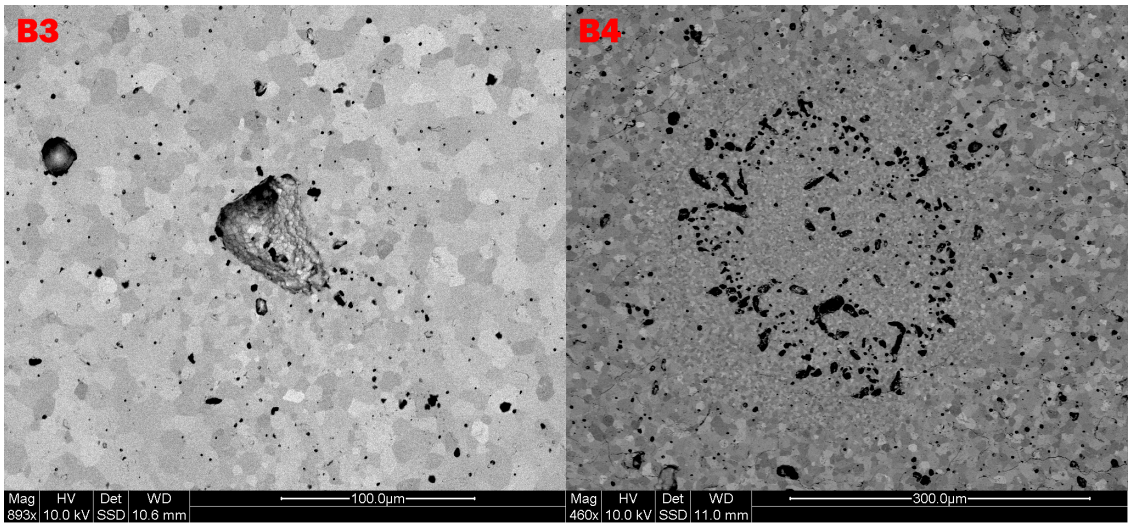

Figure 4.17: Backscattered electron SEM images of pellet B3 and R4. The images show regions of the pellets with smaller grain sizes compared to the their surroundings.

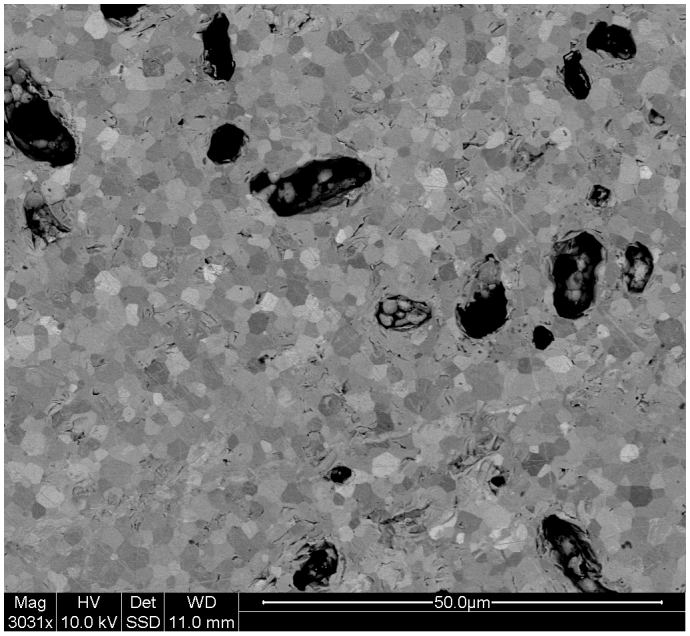

Figure 4.18: Backscattered electron SEM image of pellet B4. This as a zoomed in image of the region with smaller grain sizes in Figure 4.17 B4.

4.6.1 EDX

The EDX could, just like SEM imaging, not detect any dopant inhomogeneity. Figure 4.19 shows one line scan each from pellets B3 and B4 respectively, with the graphs showing counts per second for U, Ce and La over the line distance. Except for noise there isn't any apparent difference in cps for any of the elements. All the other line scans that were performed looked similar, only with the occasional dip in

all three elements because of pores or some kind of external contamination. The less noise in the first third of the B4 graphs are because the line scan was ran for ca. 1.3 times that run. B4 contains almost 5 times more Ce than B3, as seen in Table 4.5, but the Ce line for both elements are almost identical. Likely the amount of Ce and La in both pellets is too low for the EDX to accurately detect and measure, and the Ce and La lines are not actually representative of the real amount of dopants. Either way, if there were any larger aggregates of the dopants the EDX should be able to detect it as a larger spike in cps.

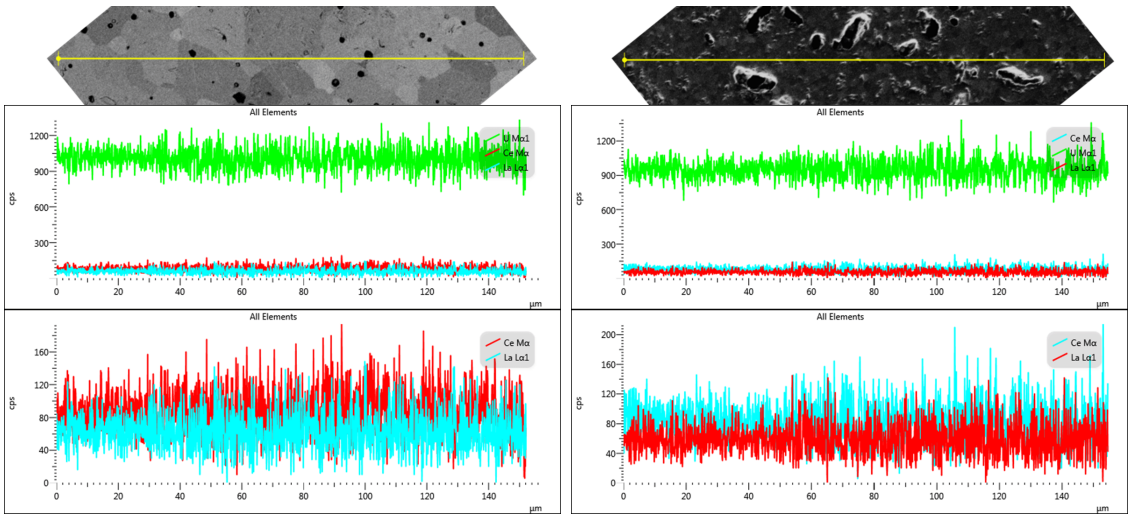

Figure 4.19: EDX line scans of pellets B3 (left) and B4 (right). Top graphs are with U, bottom graphs are only Ce and La.

Figure 4.20 shows an EDX map of pellet B3 with the distribution of Ce and La. This map also confirms the homogeneous spread of dopants.

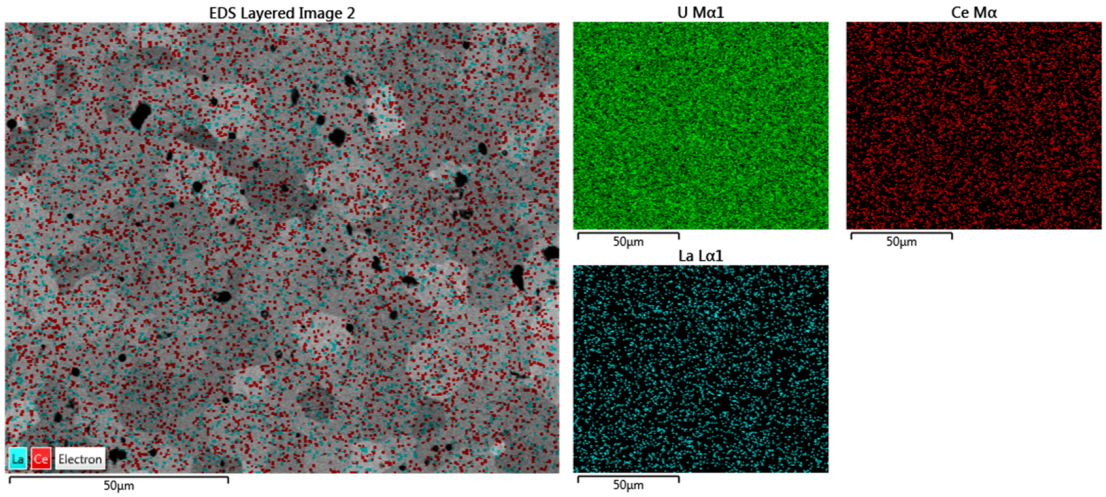

Figure 4.20: EDX map of pellet B3 showing distribution of Ce and La.

4.7 Process difficulties and suggested improvements

Written below are difficulties and setbacks encountered during the project, with suggested ways of improving the methods and avoiding the setbacks.

4.7.1 PTFE Contamination

During the making of the NM powder some unanticipated difficulties presented themselves. The one that might have had most effect on the final pellets is polytetrafluoroethylene (PTFE), or Teflon, contamination of the powders. During the precipitation of the first batch of NPs there appeared small pieces of white contaminants floating on the liquid, as seen in Figure 4.21. The right image in the figure also shows the contamination on top of the particles after filtration. The contamination was suspected to be PTFE from the stir bar but this was not confirmed and since there was no easy way to remove it the filtration continued as planned.

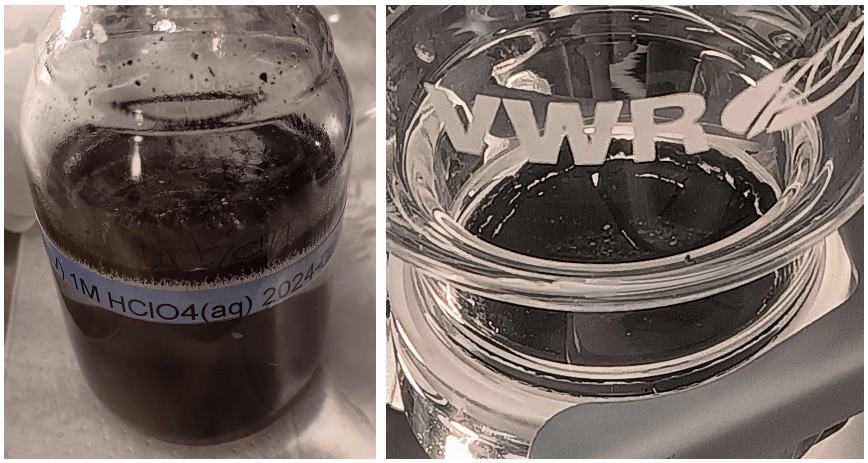

Figure 4.21: Contaminants floating on precipitation liquid (left) and contaminants on top of filtered particles (right).

There was the idea of buying a glass covered magnetic stir bar to see if that would fix the problem, but then batch 2 was precipitated without any visible contamination, so a glass stir bar was never bought. However, the third batch again got contamination during the precipitation. This time when the stir bar was inspected a flat indentation with small scratch marks could be seen, as shown in Figure 4.22. This more or less confirms that the contamination is PTFE from the stir bar which is being ground down during precipitation. Batch 2 didn't have any PTFE because unlike batch 1 and 3 it was filtered the same day as the precipitation finished, whereas batch 1 was filtered one day after and batch 3 was filtered four days after finished precipitation. The stir plate was also on during the between time, so what likely happened is that the precipitated fine aggregated UO_2 NPs acted as a sandpaper on the stir bar coating.

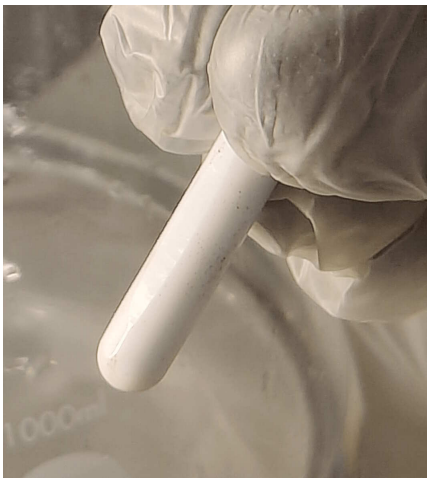

Figure 4.22: Magnetic stir bar used for the precipitation. A flat surface has formed on one part of the bar.

For batch 4 this was taken into consideration. The pH was first brought up to 2, below the limit of precipitation, in one day. But the next day there was still a small amount of floating PTFE, despite the particles still being suspended. The suspension was left without stirring for three days, precipitated fully and filtered without any additional contamination.

To easiest probable solution would be to use a glass coated stir bar instead of PTFE. It is not entirely sure that a glass stir bar wouldn't also be damaged in a similar manner, and glass fragments would be a larger concern as it could possibly be dissolved in the uranium during sintering unlike PTFE which evaporates. So testing should probably be done beforehand just in case.

If a glass stir bar is not available the best way to mitigate PTFE contamination is to limit stir speed and total stir time. When precipitating batch 3 the entire procedure was done in one day, which resulted in no visible contamination.

4.7.2 Wet powder

Even after drying for multiple days in a desiccator and the low H_2O atmosphere of the glovebox the pellets were seemingly not fully dry. The main indication for this are the large amounts of cracks in all NM pellets formed after the first sintering. The cracks most likely formed because of gas release during heating, and there are only two probable causes: water and PTFE contamination. However the PTFE contamination likely didn't contribute much to the crack formation, as B2 didn't have any visible PTFE, while still having as much cracking as B3, which had a lot of PTFE. Furthermore B4 had the least amount of cracks, and during the powder grinding step before pellet pressing the B4 powder was left ground up in the mortar for two days. This likely would have made the B4 powder much drier than the other NM powders, as water would be able to escape the small, finer powder than the larger powder aggregates. Finally a work unrelated to this thesis also looking at making pellets out of the same kind of NM powder experimentally proved that gas was released from the powder just above 100 °C. So to minimise cracking during

sintering the powder should be dried as much as possible.

The strange cracking behaviour of pellet B1 could however be because of PTFE contamination. It was the only powder with larger pieces of PTFE. B2 had non to begin with, much of the PTFE in B3 was taken out of the solution before filtering by stirring around filter papers, and B4 only had a small amount of PTFE. So B1 might have cracked the way it did because of a larger piece of PTFE inside that exploded out, creating the circular cracks. This is however only speculation.

4.7.3 Static charging

Static charging of equipment was a large problem working with the powders in the glovebox. Plastic lidded beakers were used to store the powders, which became statically charged so that powder would stick to the walls and sometimes tiny amounts would fly out of the beakers and further contaminate everything in the glovebox. When taking out small amounts of powder, e.g. for ICP measurements, the powder would fly back into the beaker if taken too close to the beaker walls. An attempt to use a standard weighing boat was made with one of the powders and when lifted up the powder exploded out over the working space, but luckily most landed on paper and could be recovered.

It is also suspected that the static electricity affected many of the results from the scale inside the glovebox, especially when weighing the powders. The cause for this concern is that holding a beaker above the scale without touching would attract it and show a negative weight of "up to" -0.1 g. Though it is unknown how much effect this actually has when the beaker is placed on the scale. Furthermore, plastic beakers could show noticeably different masses depending on where on the scale they were placed.

All things that were not plastic, like metallic spoons, the ceramic mortar and pestle, and paper tissues were expectantly not affected by static electricity. Therefor clean paper was always added when working with the powders to catch and easily add back into any beaker.

The obvious solution is to use as little plastic as possible. The only possible problem could be to find lidded glass beakers of an adequate size. The plastic beakers used were a perfect size to fit the filter cup inside, allowing the powder, together with the filter paper, to easily be added into the beaker with little spillage.

4.7.4 Counter electrode vial

When starting electrochemical reduction of batch 2 it was discovered that the counter electrode vial had been clogged. It had during the precipitation of batch 1 been kept dry in open air for around one week, which likely had caused uranium, or possibly something else from the solution, inside the glass frit to precipitate and/or aggregate, fully blocking the pores of the frit. The frit was first put in 2 M HNO_3 and ultrasonic bath, then sat in the batch 2 solution for three days which unclogged it a bit. It was then left in 8 M HNO_3 for two days which seemed to have fully unclogged the frit. After batch 2 the vial was kept in another slightly larger vial

with 1 M $HClO_4$ when the electrolytic cell was not being used, which prevented clogging.

4.7.5 Precipitation pH

As can be seen in Table 3.1, the pH values after the first addition of NH_3(aq) varies by 0.2 to 0.9 between the batches. This is because it was never decided what the first precipitation pH should have been, only a roughly somewhere between 1.5 and 2. It is possible that this could have greatly affected the size and crystallinity of the precipitated particles. Looking at the graph in Figure 2.3, the solubility limit for amorphous UO_2 lies around pH 1.5-2 at the U(IV) concentration levels of the precipitate liquid. So it is possible that at least B2 and B4 were precipitated as amorphous NPs. However, after sintering, any amorphous UO_2 would have likely turned crystalline. So the greater problem is the possibility of a particle size difference between the different batches. However, since the particle size of the powders before sintering was never measured it is not possible to know for certain how much this difference in pH affected the results.

5

Conclusion

The electrochemical precipitation route for synthesis of doped nanometric UO_2 pellets appears to be a promising method for mimicking the properties of spent nuclear fuel. The pellets have a homogeneous distribution of dopants as shown by SEM and EDX, although this was also the case for the reference pellets. Where the NM pellets lacked is in grain size, as most of the surface had a similar average size as the reference pellets. Although regions were found with grains one third the size of the bulk, close to 1 µm.

For future work the main avenue of research should be to look at alternative sintering methods to prevent or at least lower grain size growth. A logical first step would be to sinter NM pellets only at 1200 °C, possibly for longer than 4 h, and analyzing them. If they are not sintered enough then sintering temperatures between 1200 and 1650 °C could be tested to find the minimum temperature needed for adequate sintering. If the grain sizes are still suboptimal other sintering techniques should be tried, e.g. spark plasma sintering (SPS). SPS operates at lower temperatures than standard sintering, and works by applying a strong current through the conductive pressing die as the sample is pressed. The lower temperature of the SPS should lead to reduced grain growth in the pellet.

6

References

LATEX template created by: M. Gustaver (2020) A Chalmers University of Technology Master's thesis template for LaTeX. Unpublished.

[1] G. Choppin, J.-O. Liljenzin, J. Rydberg, and C. Ekberg, *Radiochemsitry and Nuclear Chemistry, fourth edition*. Academic Press, Elsevier, 2013.

[2] M. H. A. Oliva, "Preparation and characterization of fission products simfuels as a burnup analysis reference material.," M.S. thesis, IQS School of Engineering, 2021.

[3] I. Lundell and S. Ekman, "Tillverkning av kalibrerstandard för ämnesbestämning i kärnbränslen," M.S. thesis, Uppsala Universitet, 2023.

[4] IAEA, *The nuclear fuel cycle*. [Online]. Available: https://www.iaea.org/sites/default/files/19/02/the-nuclear-fuel-cycle.pdf.

[5] V. V. Rondinella and T. Wiss, "The high burn-up structure in nuclear fuel," *Materials Today*, vol. 13, no. 12, pp. 24–32, 2010. DOI: https://doi.org/10.1016/S1369-7021(10)70221-2.

[6] K. S. Mao, T. J. Gerczak, J. M. Harp, *et al.*, "Identifying chemically similar multiphase nanoprecipitates in compositionally complex non-equilibrium oxides via machine learning," *Communications Materials*, vol. 3, no. 1, p. 21, Apr. 2022. DOI: 10.1038/s43246-022-00244-4.

[7] H. Kleykamp, "The chemical state of the fission products in oxide fuels," *Journal of Nuclear Materials*, vol. 131, no. 2, pp. 221–246, 1985. DOI: https://doi.org/10.1016/0022-3115(85)90460-X.

[8] S. K. Cary, M. G. Ferrier, R. E. Baumbach, *et al.*, "Monomers, dimers, and helices: Complexities of cerium and plutonium phenanthrolinecarboxylates," *Inorganic Chemistry*, vol. 55, no. 9, pp. 4373–4380, May 2016. DOI: 10.1021/acs.inorgchem.6b00077.

[9] Analytical Sciences Digital Library, *Reference electrodes*, Chemistry LibreTexts. [Online]. Available: https://chem.libretexts.org/Bookshelves/Analytical_Chemistry/Supplemental_Modules_(Analytical_Chemistry)/Analytical_Sciences_Digital_Library/Courseware/Analytical_Electrochemistry%3A_Potentiometry/03_Potentiometric_Theory/04_Reference_Electrodes.

[10] D. Gil, R. Malmbeck, J. Spino, T. Fanghänel, and R. E. Dinnebier, "Nanoscale uo2 and novel complex u(iv)-sulphate phase formation from electrolytically reduced uranyl sulphate solutions," *rca - Radiochimica Acta*, vol. 98, no. 2, pp. 77–89, 2010. DOI: doi:10.1524/ract.2010.1694.

[11] N. Um, "Hydrometallurgical recovery process of rare earth elements from waste: Main application of acid leaching with devised τ-t diagram," in ResearchGate, Jul. 2017. DOI: 10.5772/intechopen.68302.

[12] D. Brabazon (editor), *Encyclopedia of Materials: Composites. Volume 2* (2), 1st ed. Elsevier, 2021, ISBN: 0128197242; 9780128197240.

[13] K. Khalid, R. Ishak, and Z. Z. Chowdhury, "Chapter 15 - uv–vis spectroscopy in non-destructive testing," in *Non-Destructive Material Characterization Methods*, A. Otsuki, S. Jose, M. Mohan, and S. Thomas, Eds., Elsevier, 2024, pp. 391–416. DOI: https://doi.org/10.1016/B978-0-323-91150-4.00021-5.

[14] Agilent, *An introduction to the fundamentals of inductively coupled plasma – mass spectrometry (icp-ms)*. [Online]. Available: https://www.agilent.com/en/product/atomic-spectroscopy/inductively-coupled-plasma-mass-spectrometry-icp-ms/what-is-icp-ms-icp-ms-faqs.

[15] N. Wonderling and G. Tambourine, *Density: Helium pycnometry*. [Online]. Available: https://www.mri.psu.edu/materials-characterization-lab/characterization-techniques/density-helium-pycnometry.

[16] L. E. Smart and E. A. Moore, *Solid State Chemistry: An Intruduction, Third Edition*. CRC Press, 2005.

[17] Julenkarlasaray. [Online]. Available: https://commons.wikimedia.org/wiki/File:Bragg_legea.jpg.

[18] The Materials Project. [Online]. Available: https://next-gen.materialsproject.org/materials/mp-1597.

[19] G. Leinders, T. Cardinaels, K. Binnemans, and M. Verwerft, "Accurate lattice parameter measurements of stoichiometric uranium dioxide," *Journal of Nuclear Materials*, vol. 459, pp. 135–142, 2015. DOI: https://doi.org/10.1016/j.jnucmat.2015.01.029.

[20] Y.-K. Ha, J. Lee, J.-G. Kim, and J.-Y. Kim, "Effect of ce doping on uo2 structure and its oxidation behavior," *Journal of Nuclear Materials*, vol. 480, pp. 429–435, 2016. DOI: https://doi.org/10.1016/j.jnucmat.2016.08.026.

[21] D. C. HILL, "Phase relations and crystal chemistry in the system uranium oxide–lanthanum oxide," *The American Ceramic Society*, 1962.

[22] C. Schreinemachers, G. Leinders, G. Modolo, M. Verwerft, K. Binnemans, and T. Cardinaels, "Fabrication of nd- and ce-doped uranium dioxide microspheres via internal gelation," *Journal of Nuclear Materials*, vol. 535, p. 152 128, 2020. DOI: https://doi.org/10.1016/j.jnucmat.2020.152128.

[23] WebElements. [Online]. Available: https://www.webelements.com.

[24] Nanoscience Instruments, *Scanning electron microscopy*. [Online]. Available: https://www.nanoscience.com/techniques/scanning-electron-microscopy/.

[25] R. Jovani-Abril, "Synthesis and characterization of nanocrystalline uo2 ceramics," Ph.D. dissertation, Universidade de Santiago de Compostela, 2014.

[26] D. N. French, "Grain boundaries," *The National Board BULLETIN*, 1991.

A

Additional Pellet Data

Table A.1: All pellet masses, volumes, and densities after each of the three sintering steps. TD_{UO_2}=10.96 g/cm3.

Pellet	**B1**	**B2**	**B3**	**B4**	**R1**	**R2**	**R3**
Mass before pressing [g]	0.9043	0.9150	0.9808	0.9357	0.9324	0.9077	0.8963
Mass after pressing [g]	0.8861	0.8857	0.9434	0.9008	n/a	n/a	n/a
Mass after 1st sintering [g]	0.6994	0.8087	0.8654	0.8270	0.8451	0.9038	0.8930
Volume after 1st sintering [cm3]	n/a	0.112	0.128	0.100	n/a	n/a	n/a
Density after 1st sintering [g/cm3]	n/a	7.22	6.74	8.29	n/a	n/a	n/a
TD_{UO_2} [%]	n/a	65.9	61.5	75.7	n/a	n/a	n/a
Mass after 2nd sintering [g]	0.6974	0.8069	0.8624	0.8231	0.8441	0.9030	0.8914
Volume after 2nd sintering [cm3]	n/a	0.0849	0.0838	0.0843	0.122	0.103	0.0910
Density after 2nd sintering [g/cm3]	n/a	9.51	10.29	9.76	6.91	8.74	9.83
TD_{UO_2} [%]	n/a	86.7	93.9	89.1	63.1	79.8	89.7
Mass after 3rd sintering [g]	n/a	0.8068	0.8625	0.8227	0.8439	0.9027	0.8904
Volume after 3rd sintering [cm3]	n/a	0.0836	0.0846	0.0861	0.120	0.101	0.0895
Density after 3rd sintering [g/cm3]	n/a	9.65	10.19	9.55	7.02	8.97	9.95
TD_{UO_2} [%]	n/a	88.1	93.0	87.1	64.1	81.9	90.8

B

Additional EDX scans

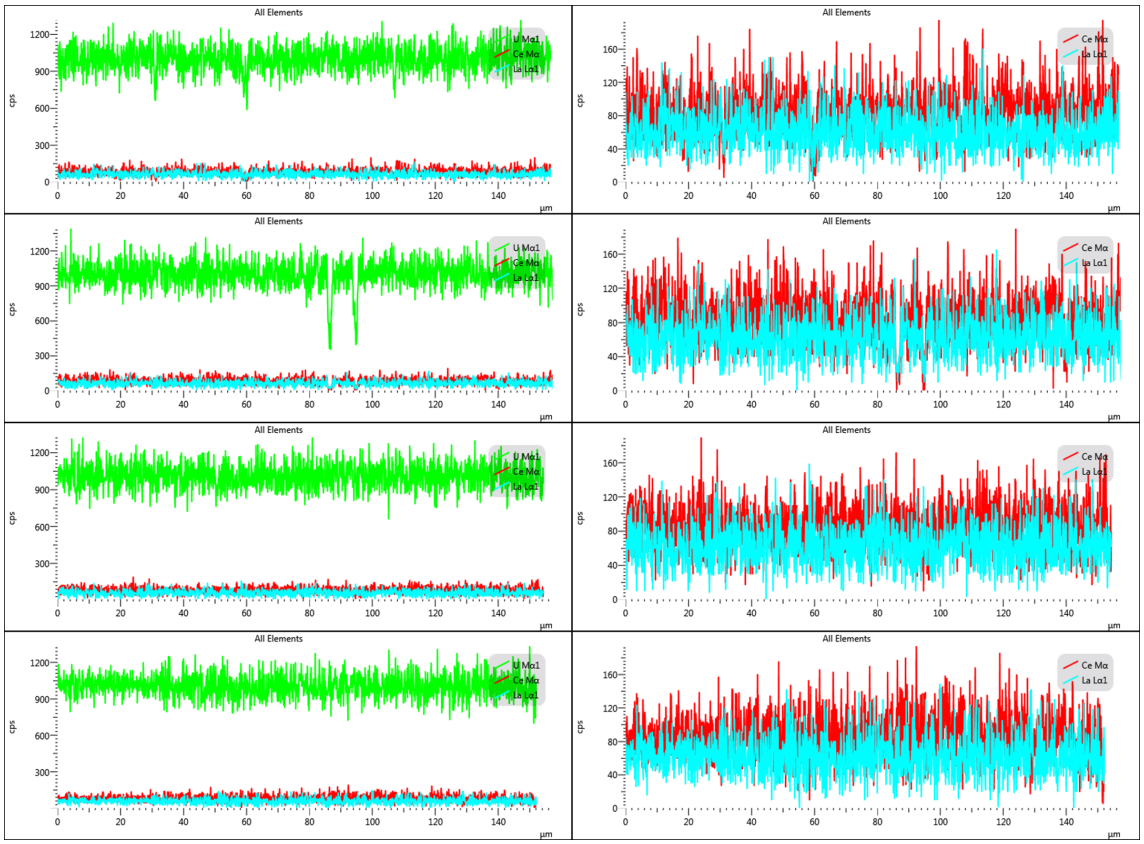

Figure B.1: All 4 B3 EDX linescans. Large drops in cps corresponds with pores in the surface for all linescans.

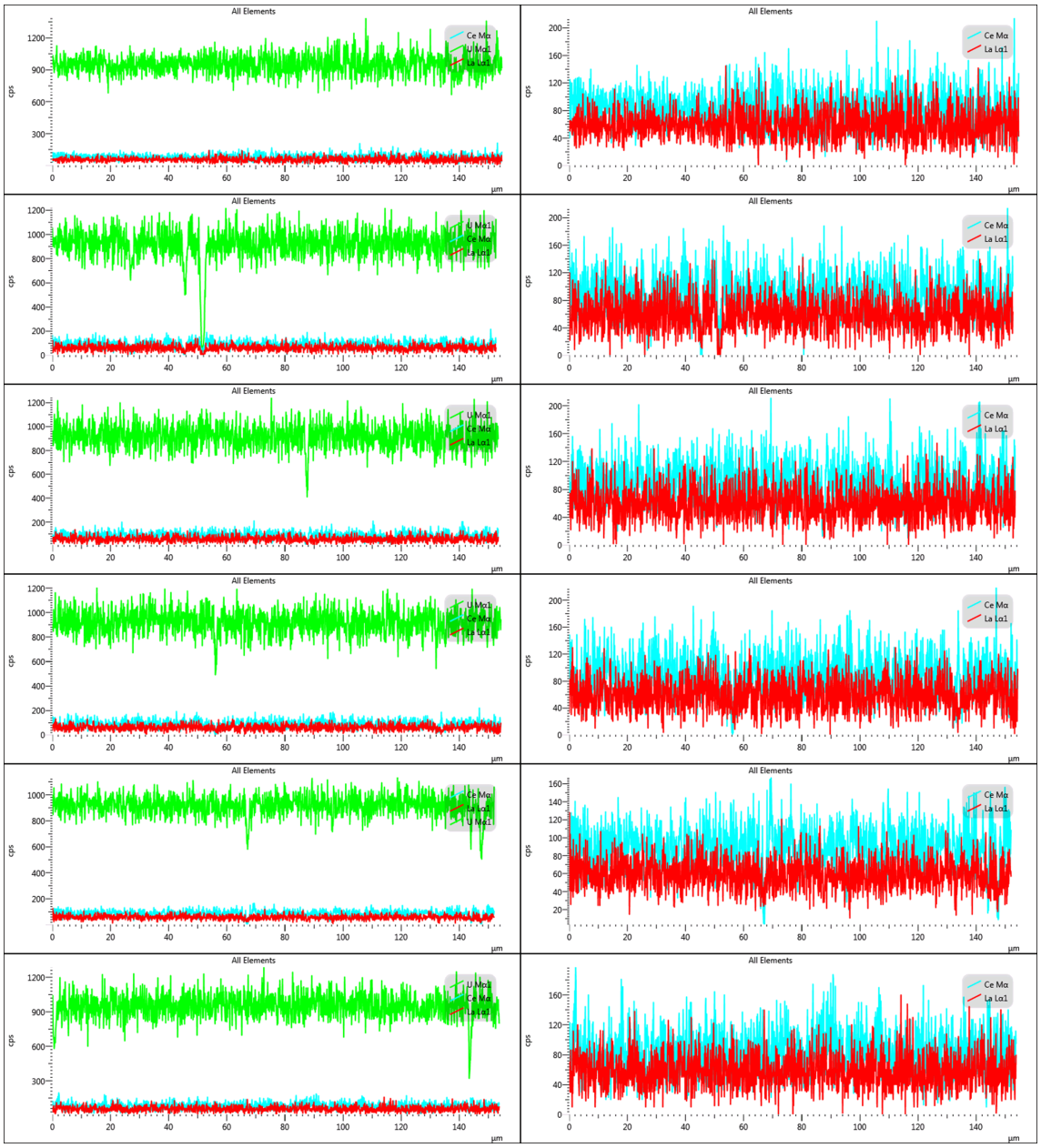

Figure B.2: All 6 B4 EDX linescans. Large drops in cps corresponds with pores in the surface for all linescans.

C

Electrolysis current graphs

Below in Figures C.1 to C.4 are shown the current over time graphs for the four electrolysis runs done on batch 4. Figure C.1 has a very peculiar shape. The spike at the end of the Figure C.2 is from the potentiostat running out of battery. The spikes in Figures C.3 and C.4 are likely from manual disturbance of the equipment.

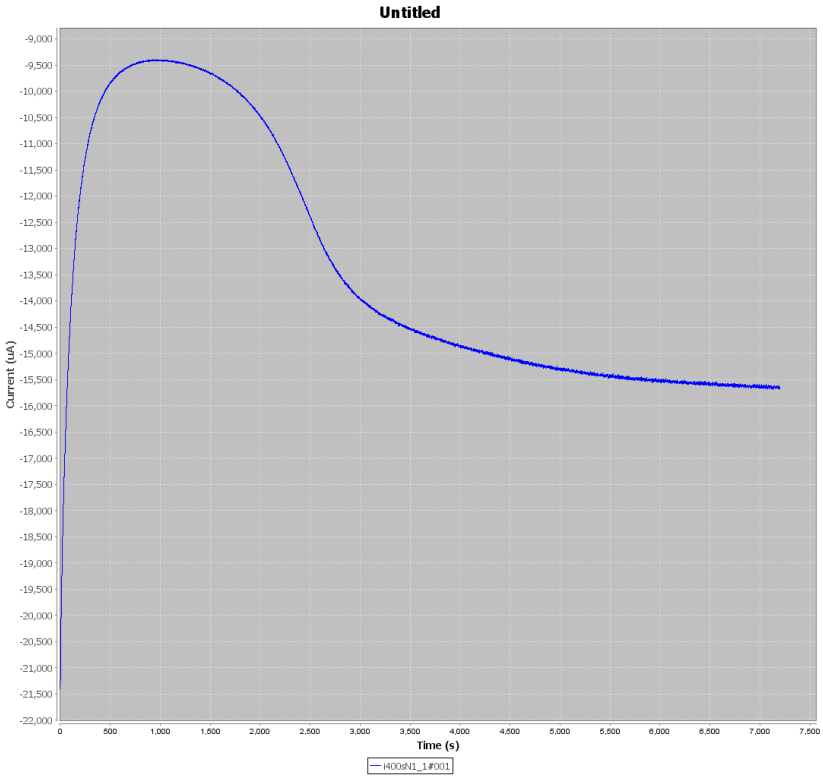

Figure C.1: Electrolysis current over time graph for batch 4, first run. Applied potential was 0.45 V.

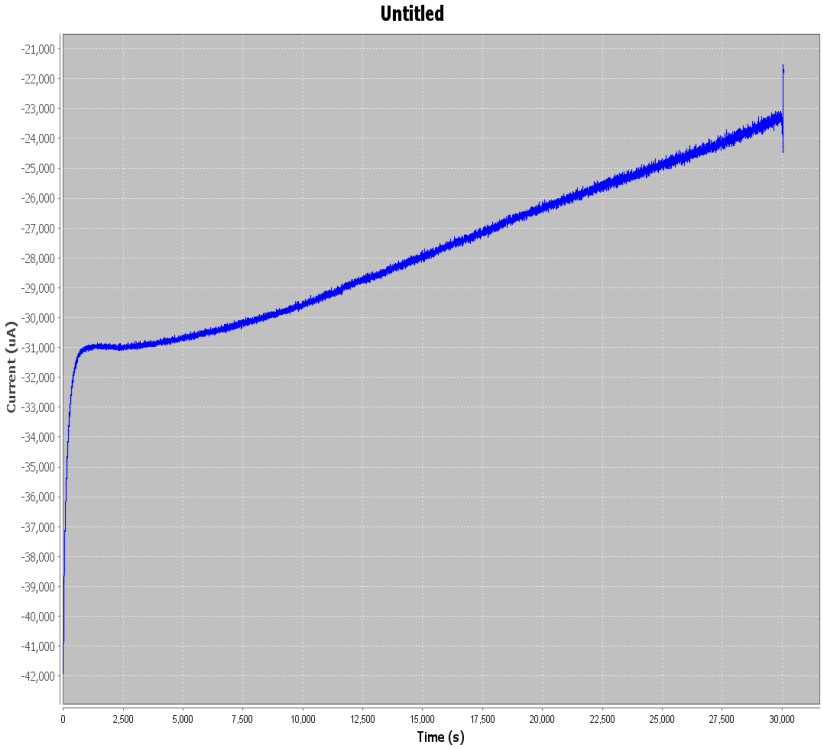

Figure C.2: Electrolysis current over time graph for batch 4, second run. Applied potential was 0.60 V.

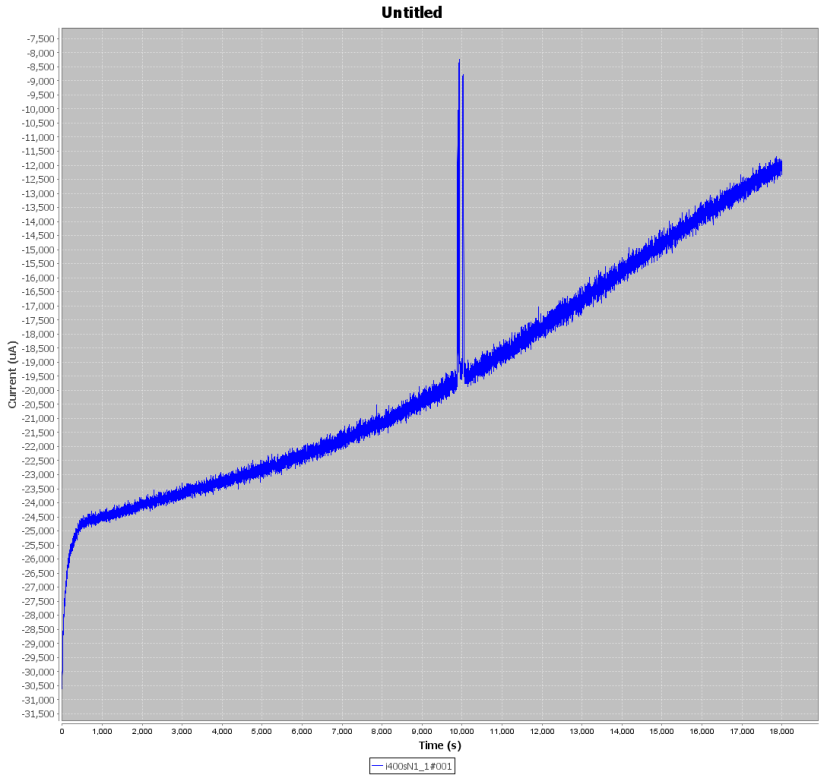

Figure C.3: Electrolysis current over time graph for batch 4, third run. Applied potential was 0.65 V.

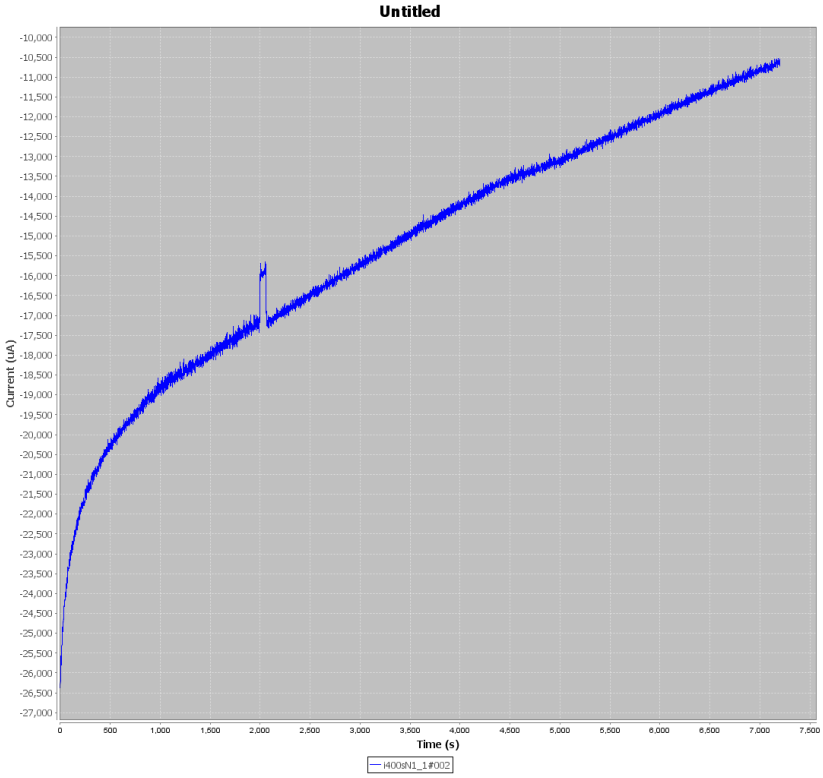

Figure C.4: Electrolysis current over time graph for batch 4, fourth run. Applied potential was 0.65 V.

DEPARTMENT OF SOME SUBJECT OR TECHNOLOGY
CHALMERS UNIVERSITY OF TECHNOLOGY
Gothenburg, Sweden
www.chalmers.se

CHALMERS
UNIVERSITY OF TECHNOLOGY